Sedimentary Geology 416 (2021) 105877

Contents lists available at ScienceDirect

Sedimentary Geology

journal homepage: www.elsevier.com/locate/sedgeo

Propagation of frontally confined subaqueous landslides: Insights from combining geophysical, sedimentological, and geotechnical analysis

M. Sammartini [a,*], J. Moernaut [a], A. Kopf [b], S. Stegmann [b], S.C. Fabbri [c], F.S. Anselmetti [c], M. Strasser [a]

[a] Institute of Geology, University of Innsbruck, Innrain 52, Innsbruck, Austria
[b] MARUM – Centre for Marine Environmental Sciences, University of Bremen, Leobener Strasse 8, Bremen, Germany
[c] Institute of Geological Sciences and Oeschger Centre for Climate Change Research, University of Bern, Baltzerstrasse 1+3, Bern, Switzerland

ARTICLE INFO

Article history:
Received 30 November 2020
Received in revised form 3 February 2021
Accepted 3 February 2021
Available online 12 February 2021

Editor: Dr. Catherine Chagué

Keywords:
Subaqueous landslides
Mass-transport deposit
Frontally confined MTD
Fold-and-thrust deformation structures
Lake Lucerne

ABSTRACT

Subaquatic mass movements are common in marine and lacustrine environments, but due to their barely predictable nature, direct observations of these processes are limited so that knowledge is only indirectly obtained by investigating the resulting mass-transport deposits (MTDs). Most research focuses on the most common frontally emergent slides, fast-moving events able to generate turbidity currents and tsunamis. Geohazards of frontally confined slides and mechanisms behind their typical fold-and-thrust deformation structures are however still poorly understood.

We investigate frontally confined MTDs in Lake Lucerne (Switzerland) by integrating bathymetric and high-resolution seismic data with geotechnical information derived from in situ Cone Penetrometer Tests and short core analysis. Investigated MTDs consist of three units: i) a mass-slide deposit, located at the base of the slope consisting of a coherent slope sequence, ii) a fold-and-thrust system developed in basin sediments, and iii) an overrunning mass flow deposit, consisting of remolded slope sediments. The deformed and thrusted basin sediments show higher undrained shear strength compared to the undisturbed basin sequence. We propose that this strengthening is caused by lateral compression leading to fluid expulsion in the high-plasticity basin sediments by the bulldozing sliding mass. Relative kinematic indicators document that the fold-and-thrust deformation structures occur rapidly. Thus, they should be considered in tsunami hazard analysis. Furthermore, our data highlight that the slope angle of the gliding surface and basin topography are key controlling factors for slope stability and propagation of basin-plain deformations, respectively. Our integrated study supports and refines propagation models proposed in marine environments, revealing the potential of investigating smaller-scale easier-to-access MTDs in lakes.

1. Introduction

Subaqueous mass movements are common processes in marine as well as in lacustrine environments, capable of mobilizing and transporting large volumes of sediments from submerged slopes to deep basins (Masson et al., 2006; Urgeles and Camerlenghi, 2013; Sammartini et al., 2019; Mountjoy et al., 2020; Strasser et al., 2020). Subaqueous slope instabilities and ensuing gravity flows represent a significant hazard to offshore and near-shore environments, being able to damage offshore infrastructures (Piper et al., 1999; Mosher et al., 2010; Carter et al., 2014; Clare et al., 2017) and to generate devastating tsunamis (Masson et al., 2006; Glimsdal et al., 2016; Watt et al., 2019; Williams et al., 2019), for which mass movements are the second most frequent trigger (Harbitz et al., 2014; Løvholt et al., 2020). Direct and real-time observations of slope instabilities are rare and challenging, and therefore, most of our understanding of subaquatic mass movement processes derives from investigating the final products of the instability process, i.e. mass-transport deposits (MTDs).

In a submarine MTD, three different domains are usually identified: the extension-dominated headwall domain, the translational domain, and the compression-dominated toe domain (Prior et al., 1984; Lastras et al., 2002; Bull et al., 2009). Frey-Martínez et al. (2006) proposed two end members in the frontal emplacement style of a deposit: i) frontally emergent MTDs, when the failing mass is able to ramp up from its stratigraphic confinement and travels downslope on the seafloor; and ii) frontally confined MTDs, in which the translating mass is buttressed against the undisturbed basin sequence (see Fig. 4 in Clare et al., 2018). In the latter type, forming the focus of this study, the toe domain is morphologically characterized by compressional ridges as superficial expression of fold-and-thrust systems, the main thrusts of which are propagating from the basal shear surface towards the top of the deposit (Frey-Martínez et al., 2006; Bull et al., 2009; Moernaut and De Batist, 2011).

* Corresponding author.
E-mail address: Maddalena.Sammartini@uibk.ac.at (M. Sammartini).

https://doi.org/10.1016/j.sedgeo.2021.105877

Frontally emergent slides are well known to be fast-moving mass-transport processes, able to generate destructive turbidity currents and tsunamis, as reported by numerous examples in the literature (Masson et al., 2002; Piper et al., 2004; Normandeau et al., 2019; Badhani et al., 2020). On the contrary, the mechanisms of frontally confined slides and related geohazards are still poorly understood, although this landslide type is increasingly identified within earlier and new published datasets (Huvenne et al., 2002; Watt et al., 2012; Strupler et al., 2017; Alsop et al., 2019). Frontally confined slides can be considered as an early stage of landslide development, which did not contain the required potential energy to ramp out and travel above the seafloor (Huvenne et al., 2002; Frey-Martínez et al., 2006). Reasons why a slide stays confined are still under debate. Some studies attest that the confined emplacement is linked to the presence of a topographical obstacle in the basin, which blocks the sliding mass and prevents further basinward propagation (Trincardi and Argnani, 1990; Callot et al., 2008). However, the presence of frontally confined slides in flat and smooth basins has led to link this frontal emplacement style to a very low slope gradient of the basal shear surface (Nugraha et al., 2020), and to a low position of the center of gravity of the failing slope mass compared to the thickness of the involved basin-plain sequence. Thus, thick slides on gentle slopes are more prone to stay confined (Frey-Martínez et al., 2006; Gamberi et al., 2011). Moernaut and De Batist (2011) confirmed this hypothesis through a statistical study of morphometrical parameters in frontally emergent and frontally confined lacustrine slides. Their analysis suggests that the depth of the basal shear surface (i.e. slide thickness) and the total height drop of the slide are the two main parameters controlling the frontal emplacement style of an MTD. Frontally confined slides are usually characterized by a lower height drop and greater depth of basal shear surface, as further supported by numerical models (e.g. Stoecklin et al., 2020). Furthermore, Puzrin et al. (2016) defined frontally confined slides as a passive and basinward-progressive failure of blocks along a distinct surface in the stable zone. Their study linked the confinement of a slide to a critical heave in the seabed level generated by each of these blocks, and to the ability of the sediments to support this step without crumbling over the undisturbed sequence and thus becoming frontally emergent.

In the last decades an increasing number of studies focused on the mechanisms of initiation and propagation of compressional deformation structures, a typical feature of frontally confined slides. Farrell (1984) proposed a model, in which the sliding mass reaches its basinward limit first and then stops generating an out-of-sequence thrusting, in which the youngest thrusts are formed more upslope. More recently, Alsop et al. (2018) highlighted that an out-of-sequence thrusting can develop even during the translation of the sliding mass, and not necessarily after the cessation of the movement of the slide front. Other studies suggest in-sequence thrusting models in which the basin sequence is progressively deformed by the vertical impact of a failing mass, and further increase of pore pressure along a distinct slip plane (Lenz et al., 2019), by a bulldozing sliding mass, propagating against the basin sequence (Frey-Martínez et al., 2006; Joanne et al., 2013; Bull and Cartwright, 2020), or by undrained loading of the basin sequence by an overrunning flow (Watt et al., 2012). Detailed outcrop-based investigations brought evidence of synchronous thrusting, where the older thrusts, instead of becoming inactive, continue to move with the younger thrusts, and therefore accumulate greater displacement (Alsop et al., 2018). In lacustrine environments, Schnellmann et al. (2005) described fold-and-thrust deformation structures of frontally confined slides using high-resolution seismic data, and linked these structures to a process of gravity spreading induced by loading of the basin sequence by transported slope material. In all these models, the deformation structures are detaching from a specific basal shear surface associated with a single or more stratigraphic horizons. The downslope extent of the failure may be prolonged and enhanced by a shear band propagation process, which is strictly linked with the shape of the slope and the strength of sediment (Puzrin et al., 2015; Stoecklin et al., 2020). The shear band initiates in the unstable zone of the slope, where the resisting forces are lower than the driving forces, and eventually propagates in the quasi-stable and stable zone, leading to catastrophic failures (Puzrin et al., 2016).

Since general characteristics of submarine MTDs, as well as their transport and initiation processes, are often comparable with MTDs in the lacustrine environment (Sammartini et al., 2019), this paper focuses on a multidisciplinary investigation of some outstanding examples of frontally confined slides in Lake Lucerne, which was already used as a case study by Schnellmann et al. (2005) for the proposed data-based conceptual model. The specific aims of this work using Lake Lucerne as a natural laboratory for studying subaquatic landslides are to: (i) evaluate which is the effect of basin-plain deformations on the geotechnical properties of the sedimentary sequence and how these properties are changing within the MTD (ii) assess the dominant mechanism initiating the basin-plain deformations, and (iii) discuss the factors governing slope stability and slide propagation.

2. Geological setting and previous studies

Lake Lucerne is a perialpine, glacially-formed lake in central Switzerland (47°N, 8.5°E), crossed by two major tectonic boundaries: the Northern Alpine thrust and the Subalpine thrust (Fig. 1). The lake consists of seven sub-basins with a maximum water depth of 214 m. The sub-basins have elongated shapes and are characterized by sharp slope breaks, dividing steep lateral slopes (ranging from 10° to 35°) and flat basin areas (Hilbe et al., 2011; Strasser et al., 2011; Hilbe and Anselmetti, 2014). This study focuses on the northern-most part of the Chrüztrichter Basin and the Küssnacht Basin as the most external basins, north of the Northern Alpine thrust (Fig. 1). These external parts are surrounded by Subalpine Molasse mountains (Keller, 2017) so that the lake substratum is also composed of molassic sandstones and conglomerates. This bedrock is covered by a glacial-to-postglacial sedimentary sequence, which reaches a thickness of up to 120 m in the basins (Finckh et al., 1984) and <8 m on the lateral non-deltaic slopes (Strasser et al., 2011).

The sedimentary sequence can be divided in three main units (Finckh et al., 1984; Schnellmann et al., 2006; Strasser et al., 2007), which are from bottom to top:

- Glacial till and glacio-lacustrine sediments deposited in sub-glacial environments, formed during the glacial retreat and sporadic episodes of glacial readvances (>17,500 cal yr BP).
- Glacio-lacustrine fine-grained detrital sediments, settled out from episodes of melt-water plumes in the Late Glacial period (17,500–11,500 cal yr BP).
- Fine-grained Holocene lacustrine sediments (<11,500 cal yr BP), dominantly derived from authigenic carbonate and biogenic production, and detrital input from small rivers and creeks.

The main part of the 120 m thick glacial-to-postglacial basin sequence consists mainly of sub-glacial and Late Glacial sediments. The Holocene lacustrine sediments with some intercalated turbidite beds and mass-transport deposits, only comprise the uppermost 5–15 m of the sequence (Schnellmann et al., 2005). On the contrary, the basin slopes are predominantly covered by a 4–5 m thick Holocene drape of hemipelagic lacustrine sediments, overlying a relatively thin Late Glacial and Glacial sequence mostly only a few meters thick above the Molassic bedrock (Strasser et al., 2007, 2011).

The MTDs occurring at different stratigraphic levels have been linked to historical and prehistorical earthquake shaking and local rockfalls in the area (Schnellmann et al., 2002, 2006). The majority of these MTDs are the result of seismically-triggered non-deltaic lateral slope failures, characterized by a translational movement along a specific stratigraphic level (Sammartini et al., 2019). In situ and laboratory geotechnical analysis carried out in Lake Lucerne (Stegmann et al., 2007; Strasser et al.,

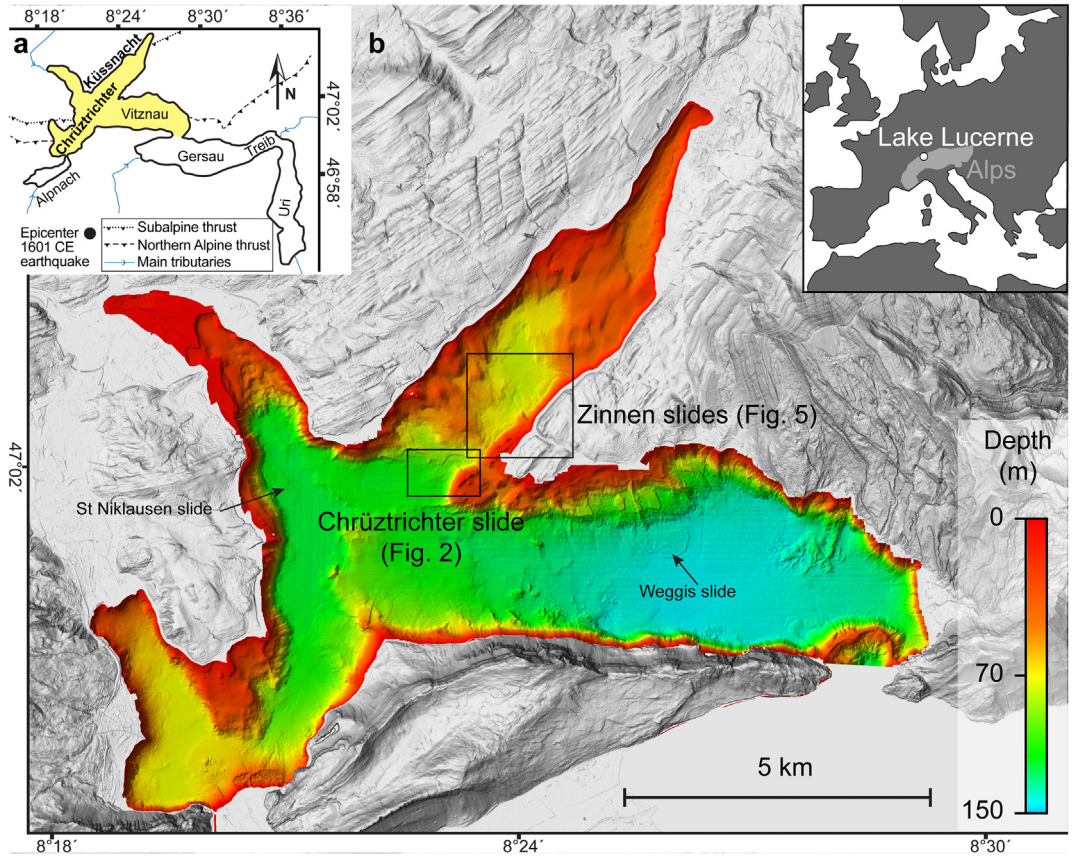

Fig. 1. a) Sketch of Lake Lucerne (central Switzerland) with its seven sub-basins, main inflows, and tectonic units (Subalpine thrust and Northern Alpine thrust). The epicenter of the 1601 CE earthquake is marked with a black dot. b) 1-m resolution bathymetric image of the three western basins, focus of this study, and shaded onshore relief (swissALTI3D hillshade, swisstopo) of the surroundings. The location of the slides discussed in this paper is highlighted with black rectangles, whereas the location of the other frontally confined slides described by Schnellmann et al. (2005) is marked with arrows.

2007) and other perialpine lakes (Strupler et al., 2017), suggests that the lake slopes tend to fail within the weak and slightly underconsolidated Late Glacial sediments immediately above the stratigraphic boundary to the underlying overconsolidated and overpressured Glacial sediments.

2.1. Previous studies on frontally confined slides in Lake Lucerne

Schnellmann et al. (2005) investigated four outstanding examples of frontally confined slides in Lake Lucerne (Weggis, St. Niklausen, Chrüztrichter, and Zinnen) with a combined seismic-stratigraphic and sedimentological approach (Fig. 1). The Weggis, Chrüztrichter and Zinnen slides were triggered by the historical 1601 CE earthquake (moment magnitude M = 5.9; epicenter location in Fig. 1a), whereas the St. Niklausen slide dates back to an even stronger prehistorical earthquake around 2200 years BP, which resulted in up to 16 landslides in the lake (Schnellmann et al., 2006; Kremer et al., 2017). In the base-of-slope area, MTDs are characterized by chaotic-to-transparent facies, which were interpreted by Schnellmann et al. (2005) as mass-flow deposit. The basinward part of the MTD comprises deformed basin-plain sediments displaying a fold-and-thrust belt style structure (Fig. 5 in Schnellmann et al., 2005). The degree of the deformation is decreasing towards the basin, and the basin-plain sedimentary sequence appears almost undisturbed at the edge of the deposit. The deeply deformed basin sequence is covered by a wedge of mass-flow deposit, visible as transparent facies on seismic data.

The conceptual model proposed by Schnellmann et al. (2005) was based on observations from seismic and core data, and assumes that the slide initiates near the headscarp and disintegrates downslope into a mass flow, which partially accumulates at the base of the slope due to a sharp break in slope gradient. The incremental loading of the lake floor induces gravity spreading and consequent deformation of basin-plain sediments. Synchronously, part of the mass flow is propagating basinward and deposits above the fold-and-thrust belt structures. Hilbe et al. (2011) added multibeam bathymetric data that supported the interpretation of Schnellmann et al. (2005) by imaging multiple deformational bulges in the near-surface Chrüztrichter slide deposit, the more buried St. Niklausen slide deposit, and the more complex Weggis area, characterized by multiple coalescing landslides and mass flows (Schnellmann et al., 2006; Strasser et al., 2011).

Nevertheless, the lack of in situ geotechnical data from basin-plain sediments so far has not allowed to test this model and its assumption from a mechanical perspective. By using an integrated geotechnical approach, this study aims at testing this in the context of the generic research questions outlined above. In particular, we focus on the hydroacoustically well-constrained Chrüztrichter slide and on the so far poorly-covered Küssnacht Basin, where new bathymetry data recently imaged multiple frontally confined MTDs (see Section 4.2). They provide an ideal natural laboratory for studying the mechanisms initiating the basin-plain deformations and the controlling factors for slope failure initiation and propagation into the basin.

2.2. Terminology

In this paper, the term *slide* is used to describe a specific instability process (i.e. Chrüztrichter slide) starting with a block of cohesive sediment sliding down the slope along a linear and inclined shear surface (Hungr et al., 2014). During the propagation, the failing mass undergoes mass and flow transformation and the event may propagate in the form of different mass-movement processes (Martinsen, 1994; Moscardelli

and Wood, 2008; Bull et al., 2009) resulting in different types of deposit. The general term *mass-transport deposit (MTD)* is hereafter used to indicate the entirety of deposits resulting from one single instability event, without built-in reference to specific gravity and/or flow processes (Pickering and Corregidor, 2005; Shanmugam and Wang, 2015; Pickering and Hiscott, 2016), with the only exception of deposits generated by turbidity currents, for which the term turbidite is used.

However, the high-resolution data presented in this study allow distinguishing, within an MTD, different deformed and/or depositional units. Therefore, for a process-related description of the MTD (see Section 5.1.2), this work refers to:

- *mass-slide deposit*: linked to the gravity-driven sliding of a coherent mass along a tilted linear shear surface and subsequent deposition (Stewart and Argent, 2000). During the lateral displacement, the coherent mass undergoes minor deformation, partially maintaining the pre-failure structure and stratigraphy. The deformed units usually fall below the lateral resolution of the seismic data (~4 m for the range of water depth of our study site) and therefore appear transparent-to-chaotic. In some cases, the internal stratigraphy of larger preserved blocks can be imaged (Martinsen and Bakken, 1990; Mohrig and Marr, 2003; Shanmugam and Wang, 2015; Pickering and Hiscott, 2016) (see Section 5.1.2.2 for details).
- *mass-flow deposit*: linked to the failing material subjected to a higher remolding, dilation, and water-incorporation with respect to the coherent sliding mass, propagating downwards as a matrix-dominated plastic flow. In seismic data, the deposit appears as a wedge-shaped basinward-thinning unit with low-amplitude, transparent-to-chaotic seismic facies (Prior et al., 1984; Schwab et al., 1996; Schnellmann et al., 2005; Moscardelli and Wood, 2008; Shanmugam and Wang, 2015).
- *fold-and-thrust system*: this deposit unit is typical of the toe domain of frontally confined MTDs and results from the compressional regime developed during the instability event. It consists of basin-plain sediments deformed along distinct shear zones. This unit appears in seismic data as deformed and displaced packages of acoustically layered sediments (Martinsen and Bakken, 1990; Schnellmann et al., 2005; Bull et al., 2009).

With the term *turbidite* we refer to a deposit generated by turbidity currents that evolved from continued water entrainment and flow transformation of the failing material during downslope movement, to form turbulent flows with low concentration of water-entrained and/or re-suspended sediment. If thick enough and thus seismically resolvable, the turbidite appears in seismic data as transparent facies on top of the MTD (Schnellmann et al., 2005; Moscardelli and Wood, 2008; Sammartini et al., 2019).

3. Methods

3.1. Bathymetric data

The bathymetric data that cover the Chrüztrichter slide were acquired in 2007 using a *Geo-Acoustics* GeoSwath Plus 125 kHz interferometric sonar (processing details in Hilbe et al., 2011). The Küssnacht Basin was mapped in 2016 using a *Kongsberg* EM2040 multibeam echo sounder with a frequency of 300 kHz (processing details in Hilbe and Anselmetti, 2014). The terrain model of the lake floor has a cell size of 1 m and the depth accuracy is in the order of few decimeters. Mapping and spatial analysis of the bathymetric data were performed using standard tools in ArcGIS 10.7 (ESRI, Inc.).

3.2. Seismic data

In order to sufficiently cover and add missing subsurface information in the newly discovered slide area in Küssnacht Basin, we added 10 km of reflection seismic lines using a *Kongsberg GeoAcoustic* Geopulse 3.5 kHz subbottom profiler (pinger). The cruise speed was maintained between 6 and 8 km h^{-1}. The theoretical vertical resolution is 10 cm and the lateral resolution (Fresnel zone) is ~4–4.5 m at a water depth of 70–100 m, respectively (Yilmaz, 2001). The software Kingdom Suite 2018 (IHS Markit, Ltd) was used for applying a bandpass filter (lower cut at 2 kHz, upper cut at 6 kHz), for seismic horizon mapping and for deposit-derived volume calculations. For the latter, the algorithm Flex Gridding was used, with a grid cell size of 5 m. The calculation was improved by adding some control points, guided by mapping of the MTD areas on the bathymetric data. A constant velocity of 1500 m s^{-1} was used for time–depth conversion. For the gliding surface slope-angle analysis (see Section 5.3.2), the picks of the acoustic basement from reflection seismic data were interpolated, creating a 5 m cell-size grid. A slope angle map of this surface was then calculated with ArcGIS 10.7 (ESRI, Inc.). Lateral shortening of the basin-plain sequence was calculated by comparing the present-day horizontal length of the fold-and-thrust system, along the slide axis, with the pre-failure horizontal length of the basin sequence. The slope-basin break before the instability event was estimated considering a slope sediment drape of ~6 m above the now-exposed acoustic substratum.

3.3. Short cores

A total of 17 short (~1.5 m) sediment cores were retrieved in 2018 using a free-fall gravity coring system. All cores were scanned with a *Geotek* Multi Sensor Core Logger (MSCL) and values of gamma-ray attenuation bulk density, P-wave velocity, and magnetic susceptibility were recorded every 5 mm. Furthermore, X-ray computed tomography (CT) scans were carried out on the most relevant cores using a *Siemens* SOMATOM Definition AS, with a voxel size of $0.1953 \times 0.1953 \times 0.3000$ mm^3. For CT scan visualization, the software VGStudio 3.3 (Volume Graphics, GmbH) and ImageJ 1.52 were used. For each location of interest, two short cores were acquired. One core for each location was split for standard geotechnical measurements (index properties: water content and Atterberg limits, undrained shear strength from fall cone tests, and grain size analysis). The water content (w) was determined by weighing ~7 cm^3 of sediment before and after drying in an oven at 50 °C, and is given as the ratio between weight of water (w_w) and the weight of dry solids (w_d) ($w = w_w / w_d$) (Craig, 2004). Atterberg limits were determined according to British Standards 1377 (BSI, 1990) using a Casagrande apparatus. The undrained shear strength from fall cone (τ_u) was measured using a 30° cone and the empirical correlation following the method by Wood (1985). Grain size analysis was performed by laser diffraction using a *Malvern* Mastersizer 3000.

The second core was kept closed as "undisturbed" whole-round sample for geotechnical testing to measure sediment-consolidation properties and shear-strength properties by oedometric and ring shear test at MARUM, Bremen. Five oedometric tests were performed on cylindrical undisturbed samples of 5 cm diameter and 1.5 cm height from different subsurface-depth levels, applying a total of eight loading steps and three unloading steps, between 2.5 and 320 kPa, following the DIN 18135 (Deutsches Institut für Normung, 1999).

Shear resistance could not be measured by standard triaxial or direct shear tests, because it was not possible to recreate the very low in situ effective vertical stress of the samples. Thus, a drained ring shear test was carried out on remolded sample using a WFI (Wykeham Farrance Intl.) *Bromhead* ring shear apparatus. Since the analyzed sediment is very loose (see Sections 4.2.2 and 5.1.1), the results obtained on a remolded sample should not differ much from the ones on an intact sample. The sediment was put in a 30 mm large and 5 mm thick ring and subjected to progressive loading increments between 2 and 247 kPa. After each consolidation and draining phase, the samples were sheared with a constant velocity of 0.002 mm min^{-1} until 3 mm displacement (DIN 18137-3, Deutsches Institut für Normung, 2002). The cohesion of the samples is calculated based on the Mohr-Coulomb failure criteria following the DIN

18137-3 (Deutsches Institut für Normung, 2002). We indicate an interval of values based on the results obtained at low normal stresses, which represent the in situ condition of our sediments.

3.4. In situ Cone Penetrometer Test (CPT)

Cone Penetrometer Test (CPT) measurements were acquired in free fall with the MARUM-developed lightweight CPT with pore pressure (SW-FF-CPTu) instrument (Stegmann et al., 2006). The probe consists of a 15 cm^2 piezocone, which, while penetrating the sedimentary sequence, is recording the cone resistance (qc), the sleeve friction (fs), and pore pressure (u2) in undrained conditions. For this acquisition, we used a 6 rod configuration with a total lance length of 7.5 m. An extra weight of 15 kg was mounted on top of the lance in order to facilitate the full penetration of the instrument. Given the very low resistance of the sediments, the sleeve friction is at its resolution limit or below it, therefore just the cone resistance was considered, from which we derived the undrained shear strength (s_u). The s_u values were calculated based on empirical equations with the measured cone resistance, and using the MSCL-derived bulk density and a standard cone factor (N_{kt}) of 15 and 17 for normally and overconsolidated clays, respectively (details in Lunne et al., 1997; Stegmann et al., 2007). The variability and influence of the N_{kt} factor on the absolute s_u values are shown in Supplementary data 1, and are considered non-critical for the further discussion within this study. Therefore, the data presented here are based on a N_{kt} value of 15. Given that the dynamic CPTu probe penetrates the sediment at velocities higher than the standard 2 cm s^{-1} (Lunne et al., 1997), a so-called strain-rate correction has to be applied to gain realistic results. In this paper we follow the method developed by Steiner et al. (2014).

To compare s_u values of sediments inside the MTD with reference undisturbed sediments in the basin and on the slope, CPT measurements were taken at reference sites and general linear trends of s_u values with depth were obtained. Percentage differences were then calculated as an average of the differences between a CPT drop within the MTD and the general reference trend below 2 m depth. By introducing this 2 m limit-depth, the post-failure sedimentation drape and the mass-flow deposit are excluded from the comparison (see Sections 5.1.2.1 and 5.1.2.2).

4. Results

4.1. Chrüztrichter slide

The Chrüztrichter slide has already been described in details based on reflection seismic and core data (Schnellmann et al., 2005) and its frontal bulge was mapped on high-resolution multibeam bathymetry (Hilbe et al., 2011). This small slide (~0.3 km^2 from headscarp to toe of deposit) detached from the north-eastern slope area of the Chrüztrichter Basin and involved 6 m of postglacial sediments. The slide scar is facing north-west, but the failing material turned counter-clockwise towards the deepest part of the basin, depositing in a south-west direction (Fig. 2). Sub-parallel arcuate compressional ridges of ~0.5 m crest-to-trough height and ~15 m spacing are visible on bathymetric data on the distal area of the deposit (0.049 km^2), which has a positive bathymetric expression of about 1.5 m.

4.1.1. Short core results

Two cores 1.4 and 1.35 m in length, were retrieved in the Chrüztrichter deposit area: 4WS18-06, hereafter termed "reference site" in the undisturbed basin, and 4WS18-05, "MTD site", in the middle of the compressional ridges area (Fig. 2; Supplementary data 2). Both cores comprise lacustrine sediments dominated by silt (always >70%), with minor amounts of clay-sized and sand-sized particles below 30% and 20%, respectively (Fig. 3). The upper 15 cm is composed of low density (~1.15 g cm^{-3}), very high water content (>450%) organic-rich sediments, with a comparably higher sand (~10–15%) and a lower clay (~10%) content, and likely links to the human-induced eutrophication of the lake in the last century (Kelts, 1978). τ_u of this uppermost interval is below detection limit.

At the reference site, the sedimentary succession comprises undisturbed cm-scale horizontal layers clearly visible on the CT scans, and shows constant density of ~1.28 g cm^{-3} with slightly higher values in the lowermost part, where thin silty detrital layers are intercalated. The core shows a water content of ~220%, and τ_u between 1 and 1.5 kPa. At the MTD-site, the top 56 cm of the horizontally-layered sedimentary succession compares and correlates well with respect to all analyzed parameters of the top 56 cm at the reference site. In contrast, the

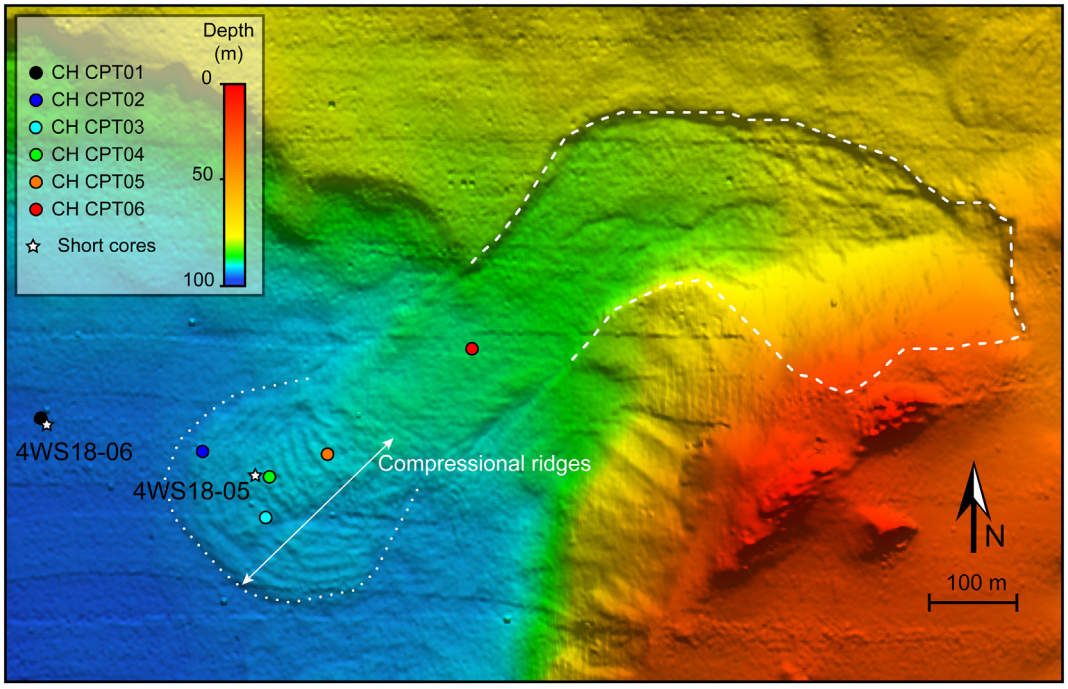

Fig. 2. Bathymetric image of the frontally confined Chrüztrichter slide, with white dashed line highlighting the headscarp and side walls of the slide, and white dotted line the frontal bulge mapped by Hilbe et al. (2011). Locations of short sediment cores and CPT drops presented in this paper are marked with white stars and color-coded dots, respectively. (For interpretation of the references to color in this figure legend, the reader is referred to the web version of this article.)

strata below 56 cm depth are composed of a 15 cm thick interval with inclined layers, overlying a distinct sand layer with increased density (1.6 g cm^{-3}) at 71 cm depth. Sediments below show soft-sediment deformation structures, such as micro faults and folds. This suggests that the MTD-site core has recovered the 1601 CE landslide feature (Schnellmann et al., 2005) at 56 cm subsurface depth, which is in agreement with the average sedimentation rate in this area (~1–1.3 mm yr^{-1}) (Schnellmann et al., 2006; Strasser, 2008). The sand layer at 71 cm depth represents a clear boundary in the Chrüztrichter MTD-site, separating two intervals with the upper 15 cm thick one showing geotechnical properties similar to the reference site and the lower, more deformed unit, displaying increased density (~1.37 g cm^{-3}) and τ_u (between 1.7 and 2.7 kPa), but lower water content (~150%). The determination of Atterberg limits highlights a plasticity index and a liquid limit of 63 and 113 in the undisturbed basin and of 47 and 91 in the MTD, respectively. These values are both in the range of extremely high-plasticity silt in the Casagrande plasticity chart (BSI, 2015) (see Section 5.1.1).

4.1.2. Cone Penetrometer Test results

Six CPT drops were acquired in the area of the Chrüztrichter slide, one in the undisturbed basin (reference site) at the same location of the reference short core described above, and five within the MTD, from the most distal area, characterized by compressional ridges, to the internal part (Fig. 2). The s_u values of all CPT drops are increasing almost linearly with depth, but with different trends (Fig. 4). The CPT drop at the reference site shows the smallest increase of s_u with depth (~0.70 kPa m^{-1}) and the deepest penetration of the lance (7 m depth). In CPT drops within the MTD, the s_u values of superficial sediments correlate well with the values of the reference site and diverge afterwards, between 1 and 1.5 m depth, showing higher absolute values and steeper trends. Taking the s_u linear increase of the undisturbed basin as reference, the average percentage difference of s_u values for each CPT drop within the MTD (below 2 m depth) varies between 17 and 52%. Both the highest and lower percentage differences are in CPT drops within the compressional ridge area, 60 m apart from each other, indicating the internal variability. The CPT drops in the more internal part of the MTD and at the edge of the frontal bulge are characterized by high (43%) and low (19%) percentage difference, respectively. Furthermore, it can be observed that, the higher the increment of s_u with depth, the lower the penetration of the CPT lance. The lowest penetration was achieved by the drop penetrating the internal part of the MTD, where the instrument reached 5.6 m depth, which is more than 1 m less than the penetration in the undisturbed basin. In almost all drops, few s_u peaks above the average linear increase (up to 3.5 kPa difference) are observed, and are most likely linked to small turbidite layers intercalated in the sedimentary sequence of the lake (Schnellmann et al., 2002).

4.2. Zinnen slides

The bathymetric data acquired in 2016 show that the Zinnen slide described by Schnellmann et al. (2005) is just one out of multiple collapses that have affected the south-eastern slope in the Küssnacht

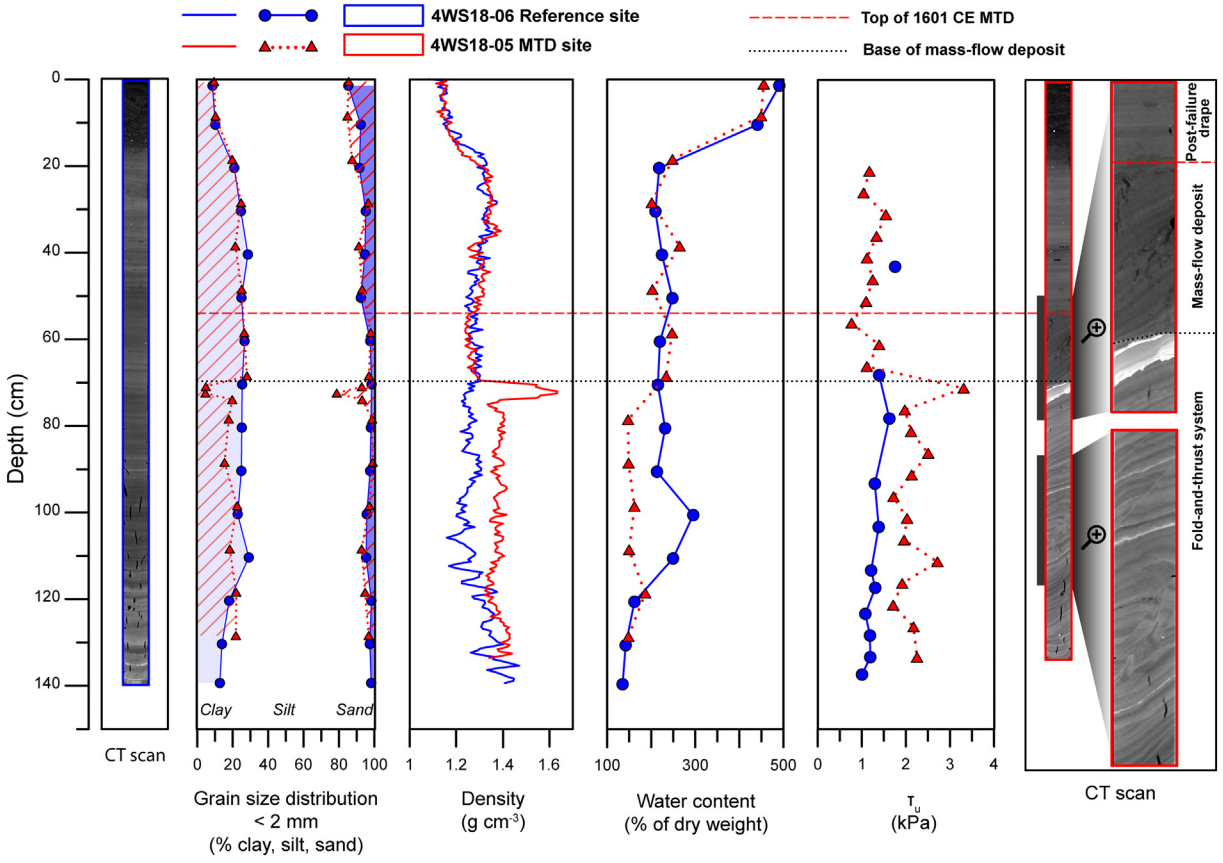

Fig. 3. Results of standard geotechnical tests carried out on Chrüztrichter short cores. In blue the results from the reference site, in red the ones from the MTD site. A horizontal red dashed line indicates the top of the 1601 CE event, which was recovered at 56 cm depth in the MTD-site core. A dotted black line indicates the base of the mass-flow deposit and therefore the top of the fold-and-thrust system at the MTD site. The mass-flow deposit shows geotechnical properties comparable with the undisturbed sequence, whereas sediments in the fold-and-thrust system show higher density, higher fall cone-derived undrained shear strength (τ_u), and lower water content compared to the undisturbed sequence at the reference site. The CT images of the two cores show horizontal layers at the reference site and soft-sediment deformation structures within the fold-and-thrust system in the MTD-site core. (For interpretation of the references to color in this figure legend, the reader is referred to the web version of this article.)

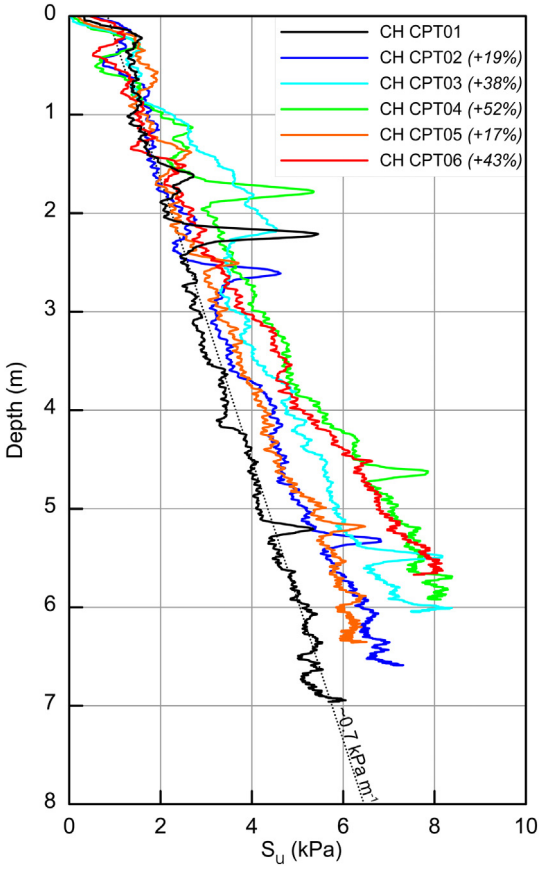

Fig. 4. In situ CPT-derived undrained shear strength values (s_u) in the Chrüztrichter area. The CPT drops within the MTD show higher absolute values and steeper trends of s_u compared to the undisturbed basin (CH CPT01). In brackets the average percentage difference of s_u for each CPT drop within the MTD in comparison to the general undisturbed trend derived from CH CPT01 (below 2 m depth), shown with a black dotted line. See Fig. 2 for color-coded position of CPT drops. (For interpretation of the references to color in this figure legend, the reader is referred to the web version of this article.)

Basin (Fig. 5). Seven different scars and related deposits can be detected in the multibeam data. Five of them show the typical features of frontally confined MTDs and overlying mass-flow deposits (highlighted with white and white-dotted lines in Fig. 5a, respectively). The two northern scars relate to more superficial slides that propagated in the basin as mass flows. Based on seismic-stratigraphic analysis, all these failures are coeval and are therefore linked to the 1601 CE earthquake (Schnellmann et al., 2005). In this study, we focus on the two central slides, Zinnen slide and Zinnen Baby slide, and on the unfailed, intact slope nearby (Fig. 5b).

4.2.1. Morphology and seismic stratigraphy

The Zinnen slide (Fig. 6a) and Zinnen Baby slide (Fig. 6b) cover ~0.1 and ~0.6 km^2, respectively, from headscarp to toe of the deposit. The average inclination of the slope is 20°, which generates a sharp break with the almost-flat basin. The headscarps are located in very shallow waters, and they are not completely visible on the bathymetric data. Nevertheless, based on the height of the side walls, the thickness of the failing material was estimated at ~6 m for the Zinnen slide, and ~5 m for the Zinnen Baby slide, involving a total volume of ~250,000 and ~83,000 m^3, respectively (Table 1). In bathymetric and seismic data, both slides show similar features and can be divided in three different sections (Figs. 5, 6).

a) a base-of-slope area where the lake floor shows convex-upward positive relief (~1.5 m) and rough surface texture compared to the smooth undisturbed basin plain, but no distinct parallel ridges (see b, below). In the subsurface, this area shows chaotic-to-transparent seismic facies (highlighted in red in Fig. 6). This is interpreted as the mass-slide deposit and will be further discussed in Section 5.1.2.2.
b) an outer area, also with positive relief in the order of 1.5 m, presenting parallel (~15 m spaced and ~0.5 m high between crest and trough) compressional ridges, perpendicular to the slide axis. On seismic data, these compressional ridges relate to thrusts, back thrusts and reverse faults dividing and displacing packages of acoustically-layered sediments forming fold-and-thrust belt deformation structures, as described by Schnellmann et al. (2005). Seismic horizons in the outer part of this deformation structure can be clearly correlated to horizons in the undisturbed basin sequence. The deformation front is characterized by a distinct steep frontal thrust (~50–60°), which divides the slide deposit from the undisturbed basin strata. A transparent seismic facies, interpreted as mass-flow deposit (highlighted in yellow in Fig. 6), overlies the deformed sediments.
c) an area where the seismically transparent facies related to mass-flow deposit, overlies the undisturbed basin sequence.

Both bathymetric and seismic data highlight that the fold-and-thrust belt deformation structures developed differently in the two slides. In the Zinnen slide, compressional ridges occur between a distance of ~125 m and ~330 m from the slope break. In the Zinnen Baby slide, the area of compressional ridges is more restricted and spans between ~70 m and ~130 m distance from the slope break.

Seismic data show that the Zinnen slide has three main thrusts (marked with black lines in Fig. 6a), two of them (at 215 m and 330 m distance from the slope break) displacing the surface and underlying packages of the basin sequence for up to 1.5 m vertically, in the outer part of the MTD. The third thrust, at 350 m from the slope break, did not reach the lake floor but was active as blind thrust just slightly affecting the basin sequence above. The position of the frontal thrust coincides with the western flank of a 100 m wide lake floor depression (with flanks of ~4° slope inclination) mimicking a depression in the underlying Late Glacial sedimentary sequence. In the Zinnen Baby slide, just one main thrust is visible on the seismic data (marked with a black line in Fig. 6b). This very steep (~60°) frontal thrust reached the lake floor at a distance of 130 m from the slope break and vertically displaced the basin sequence for ~2 m. More basinward (180 m and 240 m from the slope break), two poorly developed blind thrusts can be detected. The outer one is associated with a ramp anticline and back thrust, which folded the basin sequence above it almost up to the lake floor. All these thrusts and blind thrusts, for both Zinnen and Zinnen Baby slides, are detaching from the same stratigraphic level at ~8 m depth (marked with a dashed red line in Fig. 6). Based on seismic-stratigraphic correlation with the horizons mapped by Schnellmann et al. (2002), this decollement surface is located in the upper part of the Late Glacial sequence, ~1 m below the Holocene–Late Glacial transition (shown with a wavy gray line in Fig. 6).

The mass-flow deposit overlies the basin-plain deformation structures on both slides. In the Zinnen slide, the mass-flow deposit has a total length of 360 m and a maximum thickness of 1.5 m, and it stopped, as the deformation front, at the western flank of the glacial stratigraphic depression. In the Zinnen Baby slide, the mass flow travelled much farther than the deformation front, reaching 295 m from the slope break. The maximum thickness, in this case, is 2 m and it is reached basinward of the frontal thrust. In the base-of-slope area of both MTDs, the seismic resolution does not fully resolve the distinction between the mass flow and the underlying mass-slide deposit, but most likely is not exceeding 1 m in thickness (see Section 5.1.2.1). Considering the entire MTD, the Zinnen slide and Zinnen Baby slide deposits have a volume of 529,000 m^3 and 139,000 m^3, respectively (see Table 2).

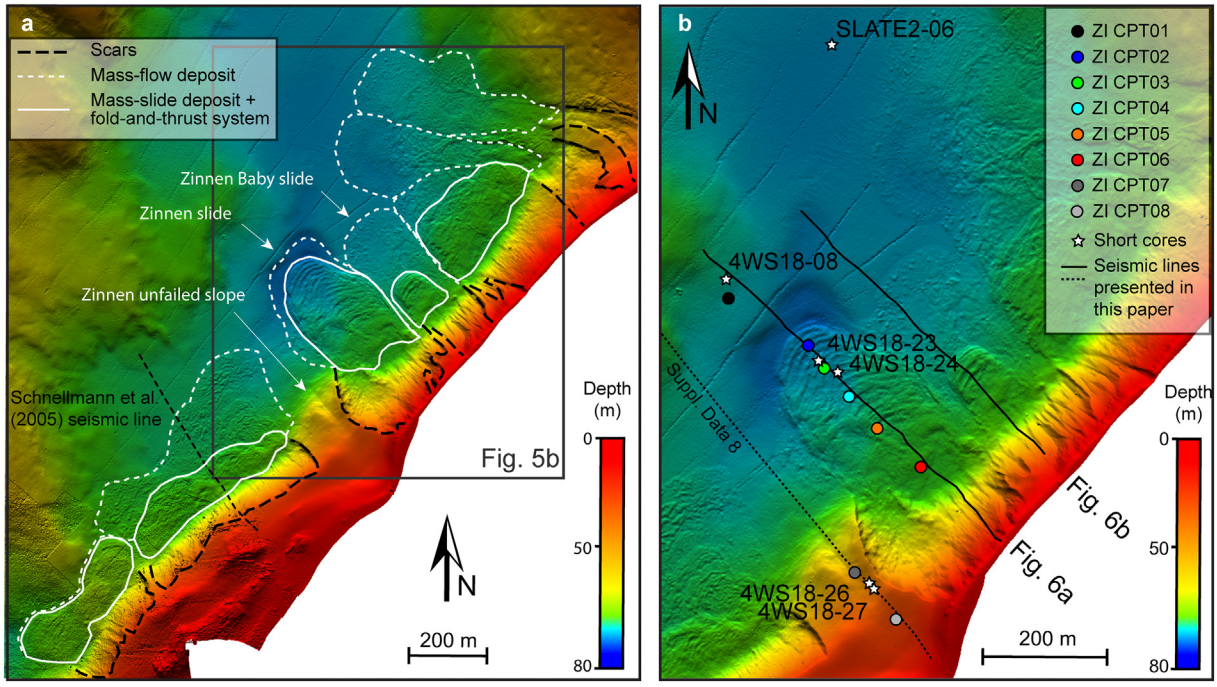

Fig. 5. a) Bathymetric image of the south-eastern slope of the Küssnacht basin, which almost completely collapsed during the 1601 CE earthquake generating multiple frontally confined MTDs. For each slide the black dashed line indicates the slide scar, white line the extension of the mass-slide deposit and fold-and-thrust system, and dashed white line the extension of the overrunning mass flow. b) Zoom-in bathymetric image of the Zinnen slide, Zinnen Baby slide, and Zinnen unfailed slope. Black lines indicate the seismic profiles presented in Fig. 6, white stars the location of short cores discussed in this paper (Fig. 7), and color-coded dots the location of CPT drops (Figs. 8, 9). (For interpretation of the references to color in this figure legend, the reader is referred to the web version of this article.)

4.2.2. Short core results

Six short cores were retrieved in the Zinnen area, two in the undisturbed basin (SLATE2-06a and 4WS18-08), two inside the MTD (4WS18-23 and 4WS18-24), and two in the unfailed slope (4WS18-26 and 4WS18-27) (see Fig. 5b for location, and Supplementary data 2 for details about each core). Fig. 7 shows the comparison between the reference 1.45 m long basin core (SLATE2-06a) and the 1.37 m long MTD core (4W18-23). The basin reference core was most likely overcored, with a loss of ~10 cm of the uppermost organic-rich sediments, linked to the human-induced eutrophication of the lake (Kelts, 1978). This interval, which in the basin core is ~5 cm thick against the ~15 cm in Chrüztrichter cores and Zinnen MTD core, is characterized by very weak sediments (τ_u below resolution) with low density (~1.15 g cm^{-3}), high water content (>450%), lower clay content (~10%) and higher sand content (~20%). Both cores show, as in Chrüztrichter, lacustrine sediments dominated by silt (>70%) and lower content in clay and sand, generally below 30% and 10%, respectively.

The reference site core comprises undisturbed horizontal layers, visible on CT scan data, with a constant density of 1.24 g cm^{-3}, an average water content of ~250% and a τ_u between 1 and 2 kPa. Between 38 and 48 cm core depth, a distinct ~10 cm thick, graded silty sand interval (55% sand at its base with higher density of 1.45 g cm^{-3}) contrasts the otherwise fine-grained layered sequence. At the MTD site, the top ~50 cm comprises undisturbed horizontal layers, which correlate with the upper ~38 cm of the reference site. Below 50 cm depth, a 2.5 cm thick interval of higher density (between 1.35 and 1.45 g cm^{-3}) sandy layers overlies a 10 cm thick interval of sediments with no internal structure. Another sandy layer at 62 cm depth divides the remolded interval from the sedimentary sequence below, which comprises layered sediments similar to the reference site, but with a slightly higher density (1.26 g cm^{-3}) and τ_u (between 1 and 2.5 kPa), and a lower water content (~200%). This lower section of the core shows subtle soft-sediment deformation structures and downcore changes in inclination and orientation of layers. This suggests that at the MTD site, the core penetrated the 1601 CE deposit at 50 cm depth, whereas at the reference site, the ~10 cm thick graded sand layer is interpreted as the turbidite linked to the same 1601 CE multi-failure event. The core acquired in the unfailed slope (4WS18-26; Supplementary data 3) highlights that the Holocene sediment drape consists here of sediments highly comparable with the upper basin sequence: silt-dominated sediments, with slightly higher density (~1.30 g cm^{-3}) and lower water content (~200%) compared to the reference site, but comparable τ_u and Atterberg limits (see results in Supplementary data 3, 4). The determination of Atterberg limits highlights very similar plasticity index and liquid limit for the three cores (63-116, 57-109, 56-107 for reference, MTD, and unfailed slope site, respectively), all in the range of extremely high plasticity silt in the Casagrande plasticity chart (BSI, 2015) (see Section 5.1.1).

Five oedometric tests were carried out in short cores of the Zinnen area, two in the basin, two in the MTD, and one in the unfailed slope (oedometric test results in Supplementary data 5). None of the five samples show evidence for an overconsolidation history and the maximum normal stress to which the sediment was subjected is coherent with the effective in situ vertical stress. The oedometric tests allowed calculating the compression index of the sediments, which is ranging from 1.62 to 2.15. A ring shear test was carried out on remolded samples from the Zinnen basin and allowed calculating the cohesion of the superficial sediments, which ranges between 1.7 and 2.7 kPa (Supplementary data 6). Given the fact that the cohesion was measured on near-surface very loose sediments, and considering that before each phase of shearing the sample has been consolidated under in situ vertical stresses, we expect that the results obtained on remolded samples are not much lower than the in situ cohesion.

4.2.3. Cone Penetrometer Test results

As for the Chrüztrichter slide, a transect of six CPT drops was acquired along the axis of the Zinnen central slide, from the undisturbed basin in front of the deposit, going into the inner, near-slope MTD (Fig. 5b). Fig. 8 highlights that in Zinnen as in Chrüztrichter, the basin CPT drop shows the lower increase of s_u with depth (~0.37 kPa m^{-1}) and one of the highest penetration of the CPT lance (7.40 m). The

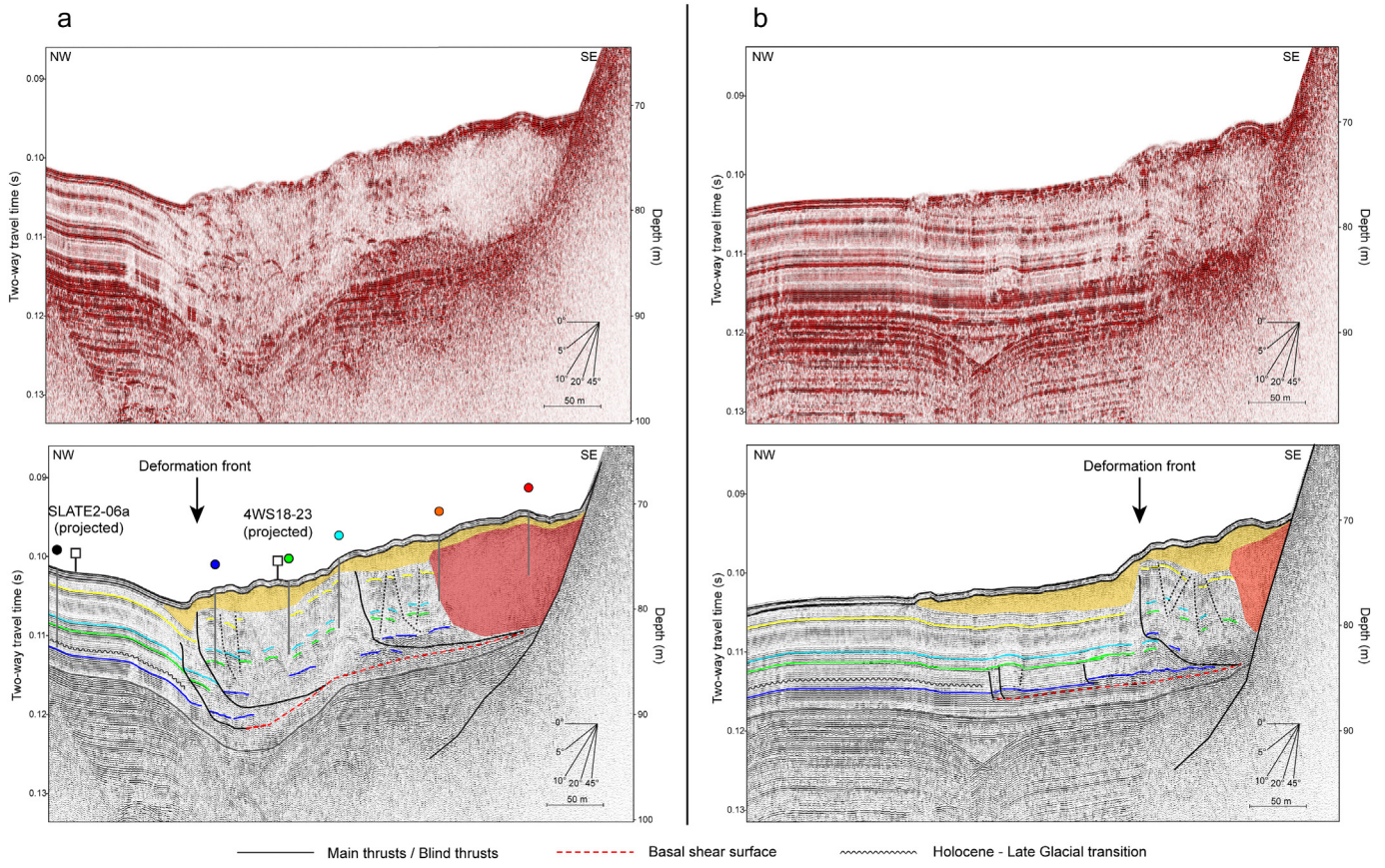

Fig. 6. 3.5 kHz seismic profiles across: a) Zinnen slide b) Zinnen Baby slide. In the interpreted profiles below, colored lines indicate seismic stratigraphic horizons in the sedimentary sequence, and the Holocene–Late Glacial transition is highlighted with a wavy gray line. The main thrusts and blind thrusts of the two slides are indicated with black lines, and detach from the same basal shear surface, marked with a dashed red line. The mass-flow deposit and the mass-slide deposit are marked in yellow and red, respectively. The projected location of the two short cores (Fig. 7), as well as the location of the CPT drops (Fig. 8) are highlighted along the Zinnen slide profile. For each color-coded CPT drop, a vertical gray line indicates the actual penetration of the CPT lance within the sedimentary sequence. (For interpretation of the references to color in this figure legend, the reader is referred to the web version of this article.)

other CPTs show comparable values of s_u in the first 1.2–1.5 m, but then different and higher trends of s_u increase are observed. The average percentage difference (below 2 m depth) of the CPT drops, compared to the linear increase observed in the basin varies from +39% in the outer part of the deposit where compressional ridges occur, to +173–176% of the two CPT drops penetrating the more internal and near-slope area of the deposit. These two CPT drops are also the ones with the lowest penetration of the instrument (~6 m), more than 1 m less than the penetration in the undisturbed basin.

Two other CPT drops were acquired in the nearby unfailed slope, at 30 and 48 m water depth (Fig. 5b). The drop in the upper slope (ZI CPT08) shows an increment of s_u with depth of ~1.08 kPa m^{-1} until 4.5 m, with some spikes exceeding the general trend by up to 6 kPa (Fig. 9a). These spikes, given the shallow water depth, can be related to more coarse-grained layers from terrestrial inputs. At ~5 m depth, s_u suddenly decreases from ~7.5, to 3.5 kPa and stays constant for 1 m and then strongly increases downcore to values up to 200 kPa where the penetration of the lance stopped (at ~5.5 m depth). In the middle slope CPT drop (ZI CPT07), the general s_u trend until 4.5 m amounts to ~0.70 kPa m^{-1}, without any spikes, indicating a more homogeneous sedimentary sequence. Between 4.5 and 5.8 m, s_u shows a constant value of ~3.5 kPa before increasing downcore to a spike of 300 kPa at 6.7 m depth, where the penetration of the lance stopped.

Table 1
Volume of slope failing mass for the Zinnen slide and Zinnen Baby slide and % of this volume which was propagating basinward as a mass flow.

Slide	Volume failing mass (m^3)	% propagating as mass flow
Zinnen slide	250,000	25%
Zinnen Baby slide	83,000	64%

5. Discussion

The new seismic and bathymetric data collected in the Chrüztrichter slide area and in the Küssnacht Basin confirmed and refined earlier descriptions of frontally confined MTDs by Schnellmann et al. (2005). These are characterized by a mass-flow deposit overlying far-reaching fold-and-thrust belt structures, which appear on the lake floor as equally spaced compressional ridges. Nevertheless, CPTs and short cores acquired inside the MTD and in the undisturbed basin nearby, for the first time, give unprecedented quantitative information on the geotechnical properties of the sediments and on how those properties are changing within the MTD. In the following sections, these data are analyzed and put together to present a new conceptual model for fold-and-thrust propagation.

Table 2
Volume of the entire MTD and of the three different MTD-units distinguished in this paper for both Zinnen slide and Zinnen Baby slide.

Slide	Volume MTD (m^3)	Volume mass flow deposit (m^3)	Volume mass slide deposit (m^3)	Volume fold-and-thrust system (m^3)
Zinnen slide	529,000	63,000 (12%)	176,000 (33%)	290,000 (55%)
Zinnen Baby slide	139,000	53,000 (38%)	30,000 (22%)	56,000 (40%)

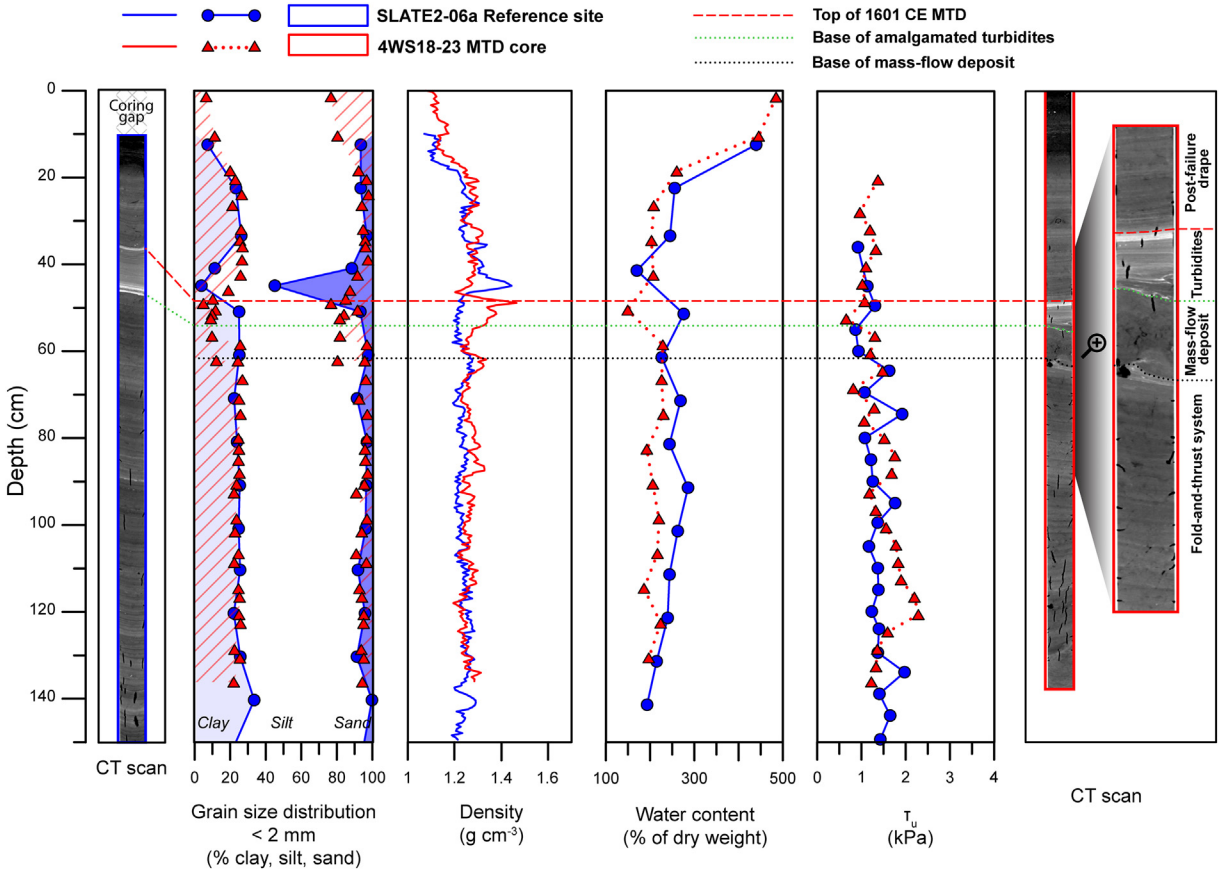

Fig. 7. Results of standard geotechnical tests carried out on Zinnen short cores. In blue the results from the reference site, in red the ones from the MTD site. A horizontal red dashed line indicates the top of the 1601 CE event, which was recovered at 50 cm depth in the MTD-site core and starts with a 2.5 cm thick interval of stacked turbidites, result of the synchronously-triggered instabilities in Küssnacht basin. The 10 cm thick mass-flow deposit is marked on top and base with a dotted green and dotted black line, respectively. Sediments within the fold-and-thrust system have slightly higher density and fall cone-derived undrained shear strength (τ_u), and a lower water content compared to the reference site. The CT images of the two cores show horizontal layers at the reference site and subtle soft-sediment deformation structures and downcore changes in inclination of layers within the fold-and-thrust system. (For interpretation of the references to color in this figure legend, the reader is referred to the web version of this article.)

5.1. Integrated characterization of the MTD

5.1.1. Sediment type

The geotechnical analysis carried out in the short cores in both Chrüztrichter and Zinnen areas shows that the basin sedimentary sequence consists mainly of silt-sized grains (>70%) that geotechnically behave like extremely high-plasticity silt as shown in the Casagrande plasticity chart (Fig. 10) (BSI, 2015). Silt is known to be non-plastic or of very low plasticity, but even a small amount of 10% clay or organic material may be sufficient to ensure the plastic behavior of the sediment (Okkels, 2019). The short distance of the measured samples from the A-line in the Casagrande chart suggests a low content of organic material and therefore a plasticity behavior linked more to the amount of clay (between 20 and 30%). The ring shear test highlighted a loose sediment characterized by low cohesion (between 1.7 and 2.7 kPa) as attested by the absence of a peak value in the shear–stress curve, which after gradually increasing to a maximum value reaches an asymptotic behavior (Supplementary data 6). Furthermore, the sample underwent an immediate reduction in volume, whereas in a structured and cohesive sediment, the sample contraction is firstly preceded by an expansion phase (Infante et al., 2016). Ikari and Kopf (2015) highlighted that, at low vertical stresses, cohesion is the dominant source of shear strength in normally-consolidated sediments, which appears to be confirmed by our data. The cohesion values are in good agreement with the fall cone and CPT-derived undrained shear strength, which in superficial sediments is ~1–2 kPa.

The high plasticity, the high water content, and the lack of internal structure of the sediment contribute to the high compressibility of the sediment (Terzaghi et al., 1996), which is confirmed by the oedometric tests and the obtained compression indexes (Supplementary data 5), ranging between 1.62 and 2.15 in Küssnacht Basin. Those values are usually higher than the ones obtained by applying an empirical correlation linking compression indexes to Atterberg limits (Supplementary data 7). The sedimentary sequence in the study area can therefore very easily be compressed, with the initial change in volume linked with the reduction in water content.

The short core analysis carried out in the unfailed slope nearby the Zinnen slide, highlights a slope sedimentary sequence highly comparable with the basin sequence, comprising high plasticity silt-sized grains. Nevertheless, the slope sediments are characterized by a slightly higher density and lower water content, which result in a higher increase of s_u with depth, as attested by the CPT data (Fig. 9a). Comparing these CPT drops with previous studies in Lake Lucerne (Stegmann et al., 2007; Strasser et al., 2007) and nearby Lake Zurich (Strupler et al., 2017), the typical mechanical stratigraphy, common for lateral slopes in perialpine lakes, can be recognized and interpreted as the following stratigraphic succession (Fig. 9a): a) the Holocene section, showing a more or less constant increasing trend of s_u, with the exception of some coarser layer-related spikes, b) the Late Glacial unit, showing low and more or less constant s_u, partly lower than the above Holocene strata, and c) the strong Glacial sediments, where the penetration of the CPT lance stopped. The slight differences in Holocene trends between the upper and middle slope are interpreted to reflect different sediment compositions: the upper slope CPT is located in a flat shallow area, where terrestrial input overtakes the lacustrine authigenic production.

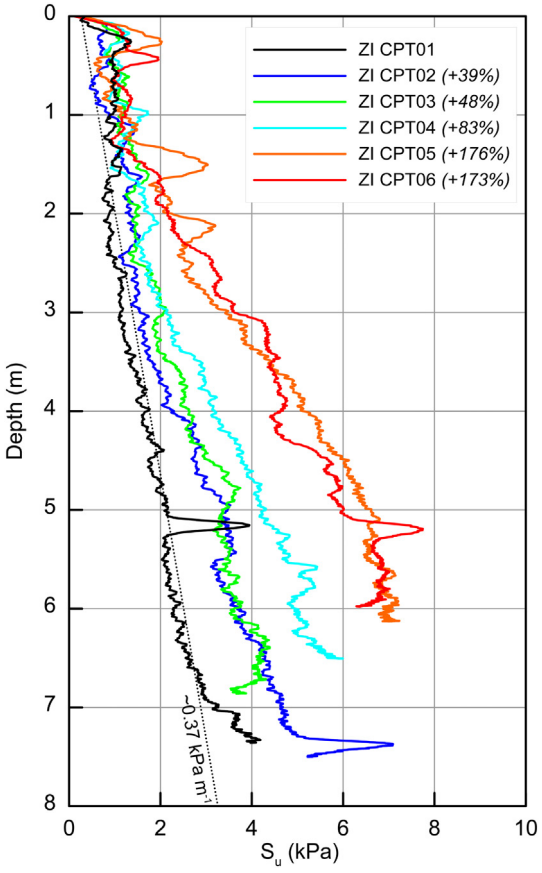

Fig. 8. CPT-derived undrained shear strength values (s_u) in the Zinnen area. The CPT drops within the MTD show higher absolute values and steeper trends of s_u compared to the undisturbed basin (ZI CPT01). In brackets the average percentage difference of s_u for each CPT drop within the MTD in comparison to the general undisturbed trend derived from ZI CPT01 (below 2 m depth), shown with a black dotted line. See Figs. 5 and 6 for color-coded position of CPT drops. (For interpretation of the references to color in this figure legend, the reader is referred to the web version of this article.)

5.1.2. MTD

As mentioned in Section 2.2, the term MTD is here used to describe the entirety of the deposit generated by a single instability event, with the only exception of turbidites. Nevertheless, the multidisciplinary approach of this study, together with the high resolution of the data acquired, allows differentiating between different MTD units, which were behaving differently during the slide propagation and deposition.

5.1.2.1. Mass-flow deposit. The mass-flow deposit forms the upper unit of the described MTDs, extending from the base of the slope over the toe of the deposit, thinning towards the basin and terminating with a distinct pinch-out point overlying undisturbed basin sediments. Both MTD-site short cores in Chrüztrichter and Zinnen recovered the mass-flow deposit, which in those locations is just in the order of tens of centimeters thick. In Chrüztrichter, the mass flow appears as a 15 cm thick package of parallel inclined layers (Fig. 3). In Zinnen the ~10 cm thick mass flow shows no internal structure and is overlain by a 2.5 cm thick package of sandy layers, interpreted here as amalgamated turbidites (Fig. 7). In an environment dominated by hemipelagic sedimentation, amalgamated turbidites are often an indication of synchronously-triggered instabilities (Van Daele et al., 2017), which is coherent with the 1601 CE multi-failure event observed in the Küssnacht Basin.

Short core analysis highlights that the mass-flow deposit has geotechnical properties comparable with the post failure sedimentation drape (Figs. 3, 7), with very high water content and low strength. This is further confirmed by the CPT drops (Figs. 4, 8), which show the same trend of s_u until ~1–1.5 m depth, i.e. the lower limit of the mass-flow deposit as identified in seismic data where the boundary between the mass-flow deposit and the underlying fold-and-thrust belt is clear and well defined. CPT drops within the MTD and their change in s_u-trend between 1 and 1.5 m depth confirmed the same thickness of the mass flow even in the inner part of the deposit, where the seismic mass-flow unit cannot be distinguished from the underlying mass-slide deposit due to similar seismic facies (yellow and red body in Fig. 6, respectively). In seismic data, the mass-flow deposit appears as a transparent-to-chaotic seismic facies (see Section 2.2), which usually indicates a great sediment disintegration with lack of coherent blocks above lateral seismic resolution (~4 m in this case study) (Watt et al., 2012). Only smaller blocks with dimensions below seismic resolution retaining intact strata occur in a mostly remolded and highly water-saturated matrix, as shown in cores from the Chrüztrichter and Zinnen mass-flow deposit.

In the fold-and-thrust system, packages of the entire involved basin sequence, i.e. from the basal shear surface to the modern lake floor, are visible below the mass flow. This suggests that the mass flow was not significantly eroding the basin sequence, which would otherwise been characterized by truncated basin sequence reflections as reported elsewhere (Joanne et al., 2013). Nevertheless, at a small scale, the short cores at the MTD sites show that the mass-flow deposit is divided from the rest of the underlying fold-and-thrust system by an erosive surface just above a sand layer that shows indications of high shear deformation in CT data (see zoom in image in Fig. 3). This indicates that a superficial erosion of sediments of the basin sequence took place during the propagation of the mass flow. These flows are known to become highly erosive when decelerating against a topographic high or at other slope-gradient breaks, with consequent incorporation of basin-floor sediments (e.g., Ogata et al., 2014). In this specific case, the mass flow most likely impacted against a package of basin sediments that was uplifted by the fold-and-thrust structures, consequently eroding and entraining an interval of loose basin sediments above a sand layer. The sand layer, characterized by a higher shear strength than the overlying silty sediments, stayed in place and acted as a basal shear zone for the mass-flow erosion (e.g., Laberg et al., 2017). In both MTD cores, the sand layer below the erosive surface has an inclination coherent with the underlying strata and therefore is considered part of the deformed basin sequence itself. The absence of this sandy layer in the reference cores confirms that it was originally located deeper than 1.5 m, i.e. the total length of the reference site cores, and that it was uplifted during the compression of the basin-plain sediments, while concurrently acting as basal shear surface of the propagating mass flow (Fig. 11c).

This superficial erosion by the mass flow has affected just the fold-and-thrust area. In the more distal part of the deposits, where the mass flow propagated above the undisturbed basin sequence, there is no evidence of erosion. This could potentially be explained by hydroplaning above a flat and smooth lake floor compared to the highly rugged basin sequence in the fold-and-thrust area (Mosher et al., 1994; Schnellmann et al., 2005).

Large parts of the mass-flow deposit consist of material collapsed from the slope, which during the downslope transport incorporated high amounts of water and a small amount of uplifted superficial basin sediments. The propagation and deposition of the mass flow were slightly delayed with respect to the propagation of the fold-and-thrust deformation structures in the basin sequence. The timing is well constrained by the fact that the mass-flow deposit i) is only superficially eroding the compressional ridge structures without flattening them, as it would have done in case of post-deformation deposition, and, ii) does not show a consistently basinward-thinning thickness, as would be expected in case of deposition above a flat surface (Schnellmann et al., 2005).

5.1.2.2. Mass-slide deposit. The mass-slide deposit is the base-of-slope unit, characterized by a rough upper surface and visible in seismic data as chaotic facies (see Section 4.2.1). The lack of laterally coherent

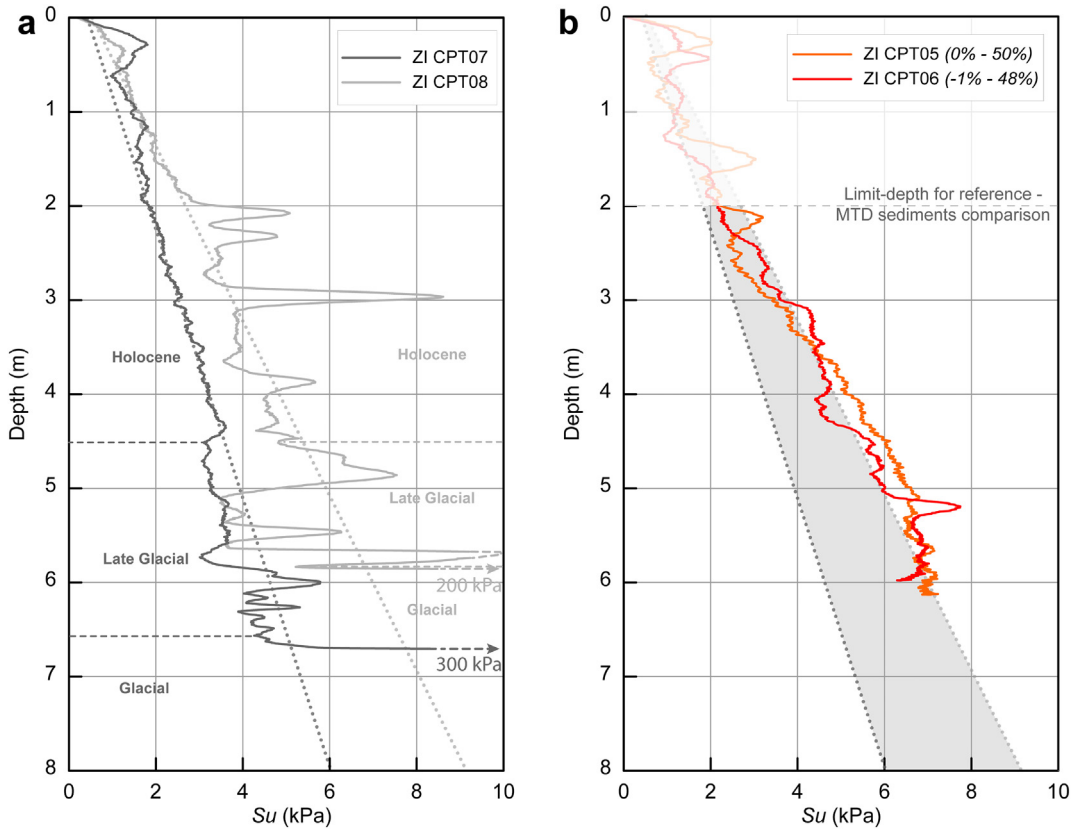

Fig. 9. a) CPT-derived undrained shear strength (s_u) in the Zinnen unfailed slope. In both middle (ZI CPT07) and upper (ZI CPT08) slope CPT drops, the typical mechanical stratigraphy of the lateral slope in perialpine lakes is recognized. From top to bottom, it consists of: Holocene package, characterized by linear increase of s_u, weaker Late Glacial sediments, and strong Glacial sediments. Dotted lines indicate the general linear trends for slope sediments. b) Comparison between the two CPT drops in the inner Zinnen slide deposit, and the general s_u range of slope sediments. In the CPT drops within the inner MTD, the average percentage difference of s_u (below 2 m) shows no variation or a slight increase of s_u when compared with the upper and lower limit of the s_u range of slope sediments.

reflections is usually one of the main criteria for distinguishing failed from unfailed sediments and suggests the presence of remolded, highly distorted sediments, or intact blocks below seismic resolution (Damuth, 1980). Nevertheless, coherent and undisturbed packages of sediments have been documented in the inner part of the frontally confined St. Niklausen slide (Schnellmann et al., 2005), as well as in other seismically chaotic submarine deposits (Jackson, 2011; Badhani et al., 2020). This suggests that the sediments of a chaotic seismic facies are not necessarily completely remolded and can still maintain their internal structure even after significant transport. The absence of high-amplitude reflections in seismic data, instead, could be linked to internal heterogeneity of the deposit, discontinuous reflectors, and to the presence of internal deformation structures that are below the lateral seismic resolution (Ford and Camerlenghi, 2020). The hypothesis that this

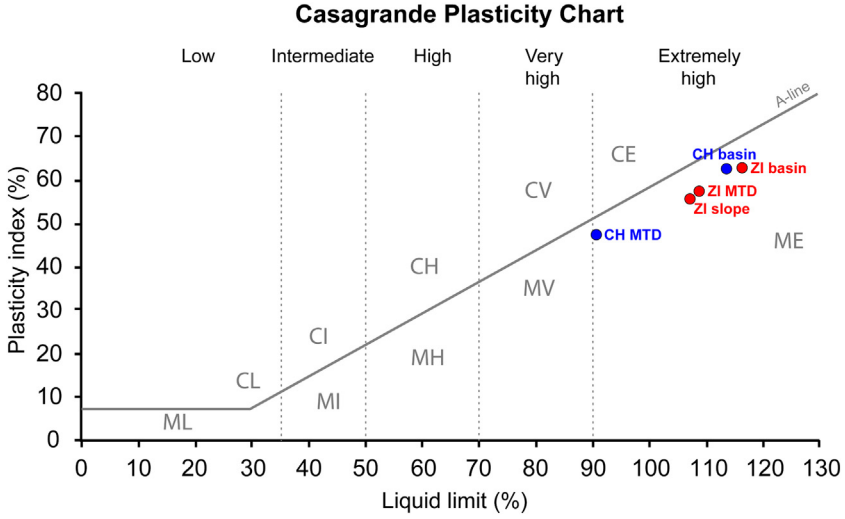

Fig. 10. Casagrande Plasticity Chart (BSI, 2015) with results of the Chrüztrichter (CH) and Zinnen (ZI) cores. This chart classified the sediment based on the geotechnical behavior and it is not necessarily providing grain-size information. The empirical A-line divides silt (M) from clay (C). Based on the plasticity the sediment is classified as: L: Low plasticity; I: intermediate plasticity; H: high plasticity; V: very high plasticity; E: extremely high plasticity.

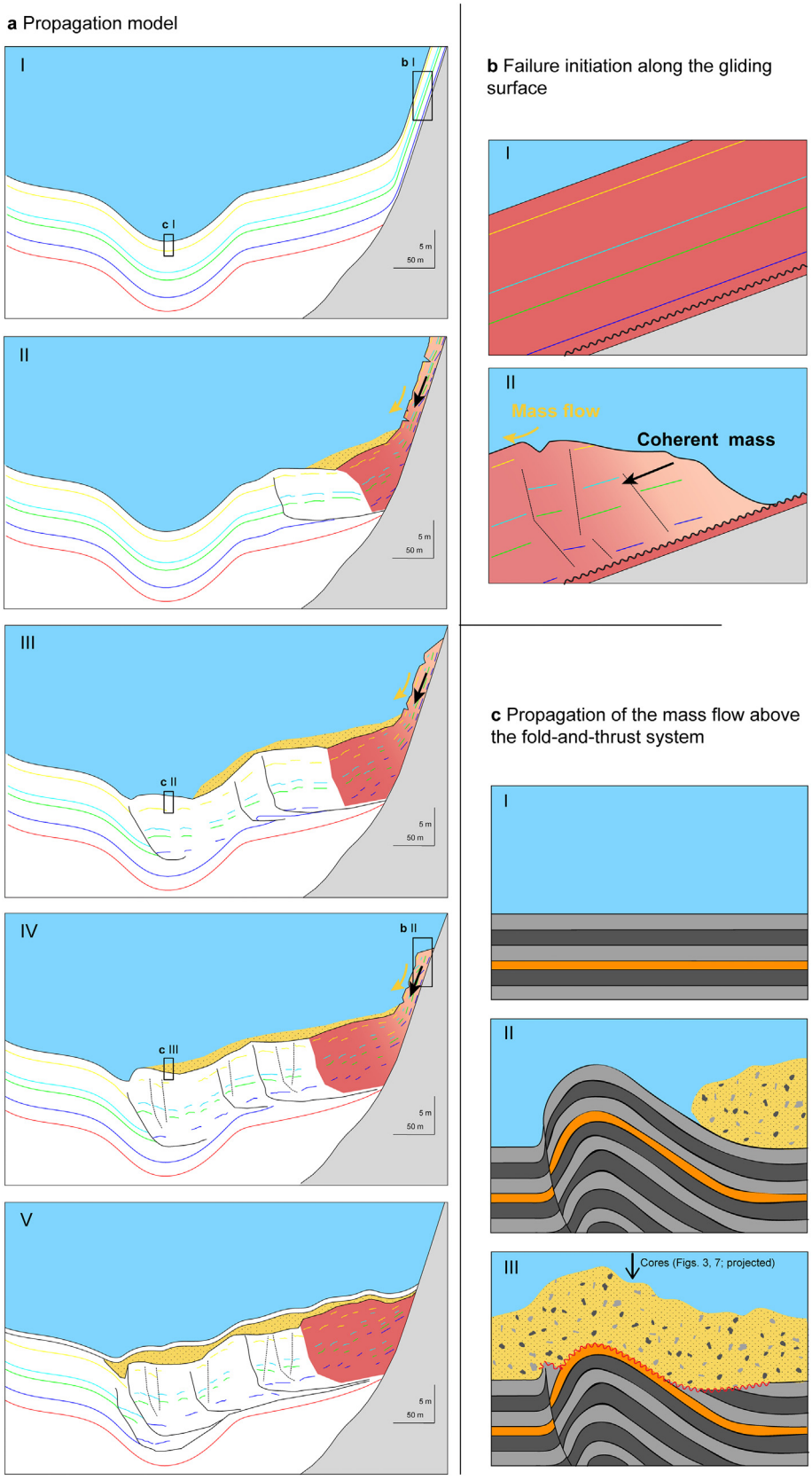

Fig. 11. New conceptual model for the propagation of fold-and-thrust structures in the toe region of frontally confined slides. (a) Schematic model as deduced from the Zinnen slide, Lake Lucerne. (b) Zoom on the slope. The slope sequence gets destabilized by the earthquake and starts to slide along a specific gliding surface (marked with black wavy line). The sliding mass is divided in blocks of intact sequence by shear strain surfaces. The upper part of the sequence disintegrates and mixes with water, propagating as mass flow. (c) Zoom on the propagation of the mass flow above the fold-and-thrust structures. The mass flow is slightly delayed with respect to the propagation of the deformation, and superficially erodes the emerging bulges along a stronger sandy layer. The erosional surface is marked with a red wavy line. (For interpretation of the references to color in this figure legend, the reader is referred to the web version of this article.)

Table 3
Volume compression and lateral shortening of the basin-plain sequence due to lateral compression by the bulldozing slide mass for both Zinnen slide and Zinnen Baby slide.

Slide	Volume pre-compression basin-plain sequence (m^3)	Volume post-compression basin-plain sequence (m^3)	Volume compression (%)	Lateral shortening (%)
Zinnen slide	343,000	290,000	15%	32%
Zinnen Baby slide	75,000	56,000	25%	43%

near-slope body is an internally-deformed but coherent mass-slide deposit and not a remolded mass-flow deposit, is confirmed by CPT data. In both Chrüztrichter (CH_CPT_06 in Fig. 4) and Zinnen (ZI_CPT_05 and ZI_CPT_06 in Fig. 8), the data highlight a stronger sedimentary sequence than the CPT data of undisturbed basin sediments, mass-flow deposits and more distal fold-and-thrust systems. In particular, in Zinnen, the two CPT drops show a very high average percentage difference from the undisturbed basin trend (176% and 173%).

In Lake Lucerne as well as in other perialpine lakes, translational slope failures occur along a gliding surface within the fine-grained Late Glacial package, above the stronger, coarser, and overpressured glacial sediments (Strasser et al., 2007; Strupler et al., 2017). The Late Glacial package on the Lake Lucerne slopes is very thin (1–2 m maximum), so the failing materials consist mainly of Holocene sediments (~4–5 m thick). Comparison of the two inner CPT drops in the Zinnen slide with the general trend of s_u in the Holocene package derived from the unfailed slope CPT drops (Fig. 9b) highlights that the sediments in the inner MTD show no variation (~— 1–0%) or a slight increase (~48–50%) of s_u values when compared with the upper and lower limit of the s_u-range of slope sediments, respectively.

These in situ s_u values support our interpretation that the base-of-slope area of the frontally confined MTDs consists of transported slope material. This material slides as a coherent mass along the translational gliding surface plowing into the base-of-slope basin-plain sediments, where it only partially experiences internal deformation and compression. However, it transfers significant compressional stress to the basin sequence, generating a propagating fold-and-thrust deformation belt (Fig. 11a and Section 5.1.2.3). During the downslope transport, the slope material may undergo strength reduction, with shear strain surfaces dividing blocks of intact slope sequence. Nevertheless, this strength reduction may be compensated by lateral compaction due to buttressing against the basin-plain sequence. Moreover, during the ~400 years of post-failure burial, the mass-slide deposit may have increased its shear strength as a consequence of porosity reduction due to shear compaction and clay-fabric alignment, to which the material was exposed during failure (Cardona et al., 2016; Moernaut et al., 2020). This could potentially explain why the mass-slide deposit shows similar trend and values of s_u of the sediment in the unfailed slope (Fig. 9b).

5.1.2.3. Fold-and-thrust system. This unit of the MTD is characterized by far-reaching fold-and-thrust deformation structures, which are a striking characteristic of frontally confined slides (Schnellmann et al., 2005; Frey-Martínez et al., 2006; Moernaut and De Batist, 2011). Previous studies highlighted that the fold-and-thrust area consists of deformed basin-plain sediments rather than slope sediments (Huvenne et al., 2002; Watt et al., 2012). This is confirmed by the seismic data that show blocks of the basin sequence with coherent internal reflections divided by seismically transparent-to-chaotic zones, along which the shear strain was focused during the deformation as reported elsewhere (Joanne et al., 2013). The amplitude and the continuity of seismic reflections in the fold-and-thrust system are increasing towards the basin, pointing to a higher preservation of the basin-plain sequence and therefore to a lower degree of sediment deformation in the toe region of the deposit (Gamberi et al., 2011; Watt et al., 2012; Joanne et al., 2013). While above-mentioned studies are based on seismic data analysis alone, our investigation adopts an integrated approach of reflection seismic data, sedimentological and geotechnical core analyses, and in situ CPT data, allowing to test these interpretations.

At both Chrüztrichter and Zinnen, the short core at the MTD site penetrated the area of fold-and-thrust structures below the mass-flow deposit, from which they are divided by an erosive surface. In Chrüztrichter, the deformed unit is characterized by higher density, lower water content and higher τ_u values when compared to the undisturbed sequence of the reference site, indicating that compression and deformation of the basin sediments led to a loss in water content and consequent increase in strength. Lateral compression is also suggested by the presence of micro-deformation structures such as faults and folds observed in the CT scans, the orientation of which are all coherent with one principal direction of shearing. In contrast, the deformed sequence cored at the Zinnen MTD site shows only a few blocks with higher density, lower water content and higher τ_u, indicating a less deformed basin sequence in comparison to the one cored in Chrüztrichter. A low compressional deformation in this upper part of the Zinnen fold-and-thrust system is also suggested by the lack of clear soft-sediment deformation structures in the CT scan. This is also supported by the oedometric tests (Supplementary data 5) showing that the maximum normal stress the sample was subjected to is between 2.5 and 5 kPa, which is consistent with a sample depth of ~1.20 m in normal consolidation state. Comparing the s_u trends between MTD and reference sites for the deeper subsurface and the more internal part of the fold-and-thrust system, indicates that the internal compression of the basin-plain sequence is higher in the Zinnen slide (percentage increase of s_u within the compressed fold-and-thrust system ranges between 39% and 83%) than in the Chrüztrichter slide (17% to 52%). This is interpreted to be the result of weaker, and therefore easier to compress, sediments in the Küssnacht Basin (increment of ~0.37 kPa m^{-1} at the reference site) compared to the Chrüztrichter Basin (increment of ~0.70 kPa m^{-1} at the reference site).

The CPT transects across the two slides show general trends of decreasing compression from the internal part to the more external part of the fold-and-thrust system. This suggests that the external basin sediment, which has been thrusted and uplifted along the frontal thrust, was less compressed and strengthened than the more internal basin sequence, proximal to the mass-slide deposit. A similar deformation trend of the basin sequence was also reported by an outcrop-based investigation of fold-and-thrust systems, which highlighted that deformation and lateral compaction are higher in the central part of the deposit (shortening of up to 50%), where the thrusting first initiated, and diminish towards the toe of the deposit (shortening under 10%) (Alsop et al., 2016). As inferred from the results from the short cores, the strengthening of the sedimentary sequence in the fold-and-thrust area can be linked to their compression and consequent loss in water content. Lateral compression is also inferred from structural interpretation of seismic data where packages of basin sediments inside the deformed area show the same vertical thickness of the equivalent undisturbed basin sequence. In the simplest case of the Zinnen slide, and assuming pure lateral compression induced by the plowing slide mass (Fig. 11a and see conceptual model in Section 5.2), the basin-plain sequence underwent a lateral shortening of ~32% compared to the pre-failure horizontal length (Table 3). Moreover, the lateral shortening allowed the coherent sliding mass to propagate and deposit at the base of the slope.

The extremely high-plasticity basin sediments with high compression index (see Section 5.1.1) must have facilitated plastic deformation during lateral compression. The sediments exhibit a plastic behavior for a wide range of water contents and therefore a wide range of depths, allowing the formation of thick fold-and-thrust structures. This is also indicated by regular and positive-relief ridges perpendicular to the slide movement direction as observed in bathymetric data. These are the superficial expression of the large-scale plastic deformations in the basin-plain sequence, confirming that the sediments behaved as a coherent high-plasticity mass (Lastras et al., 2006). The thrusting of the

basin-plain sequence followed an in-sequence propagation, with the youngest thrusts developing in the footwall of older thrusts. The older thrusts kept moving even after the nucleation of the younger thrusts, accumulating greater displacement during synchronous thrusting (Alsop et al., 2018). The basinward synchronous propagation of the deformation front is confirmed by: i) blind thrusts in front of the Zinnen slides, basinward of the main frontal thrust marking the position where the next thrust would have formed (Nugraha et al., 2020); ii) the basinward decrease of degree of deformation of the basin-plain sediments, with a more preserved internal structure in the toe region (Gamberi et al., 2011; Watt et al., 2012; Alsop et al., 2018); and iii) the same height of all the thrusts, without enhancement of any individual thrust displacement, which would be typical of out-sequence thrusting (Frey-Martínez et al., 2006; Alsop et al., 2018). Alsop et al. (2020) presented the possibility of significant back-collapse of thrusts shortly after their formation, in which the extensional reactivation of the faults may result in a partial, full, or over compensation of the thrust displacements. In our case study, if this process was present, it would not be relevant enough to obliterate the morphological expression of the thrusts, which appear as 0.5 m high ridges on the present-day bathymetry.

As in other frontally confined MTDs with internal fold-and-thrust systems (e.g., Frey-Martínez et al., 2006), the deformation is rooted in a basal shear surface, which is conformable with the surrounding strata and represents a distinct stratigraphic horizon. The location of such a decollement surface is usually strictly linked to the variation of geotechnical properties in the sedimentary sequence, and in particular to layers with induced or inherited reduced shear strength and/or excess pore pressure (Locat et al., 2014; Gatter et al., 2020). In the Chrüztrichter slide, seismic data pinpoint the decollement surface within the Late Glacial deposits. The presence of a 1 m thick highly deformed zone below the fold-and-thrust deformation structures (Schnellmann et al., 2005) suggests that the decollement surface occurs in a zone more than in a single layer. In both Zinnen slides, the decollement surface is located at the same stratigraphic level within the upper Late Glacial sequence, which also stratigraphically correlates to the basal failure surface of the slide mass on the slope. The latter develops in the upper part of the slightly underconsolidated Late Glacial sequence, characterized by low s_u values (Stegmann et al., 2007; Strasser et al., 2007; Strupler et al., 2017) (see Section 5.1.2.2). Therefore, we interpret the decollement surface to be a continuous "weak layer" from the slope to the basin sequence, allowing the initiation of a shear band in the steepest part of the slope and its propagation into the stable basin zone (Supplementary data 8). This results in longer failures and in the deformation and shearing of otherwise stable sediments in the basin, as supported by numerical models by Stoecklin et al. (2020).

5.2. Slope failure and slide propagation: a new conceptual model

Based on the results and derived process-based interpretation presented above, and taking the Zinnen slide as main case study, a new conceptual model for the propagation of basin-plain deformation structures is proposed (Fig. 11a).

The slope sequence, destabilized by an external trigger (an earthquake in this case study), starts to fail along a specific stratigraphic level (in this case study within the upper part of the mechanical weaker Late Glacial sediments) and evolves as two different bodies (Fig. 11b):

a) the weak and water-saturated upper strata, due to shear stress with the inert water column, disintegrate and mix with water, moving downslope as a remolded mass flow, forming a body still sediment-dominated but with a very high water content (yellow body = mass flow in Fig. 11a).
b) the deeper strata behave as a coherent sliding mass, accumulating some internal deformation during the downslope movement, and plow into the basin-plain sediments (red body in Fig. 11a).

The coherent sliding mass acts as a bulldozer adding lateral compressional stress to the basin-plain sediments initiating in-sequence synchronous thrusting of the basin sequence composed of sediments with a high water content and high compressibility. Basal shear along the decollement is facilitated by shear band propagation along the same stratigraphic "weak layer" that acted as failure plane on the slope. Evolving in-sequence synchronous thrusts detach from this decollement surface and propagate upwards to bulge the lake floor, uplifting and laterally compressing packages of basin sequence. These far-reaching fold-and-thrust structures form a series of compressional ridges as typical morphological expression of such frontally confined slides. The basinward-propagating failure of basin sediments stops when the lateral stress imposed by the sliding mass becomes lower than the resistance of the basin sequence (Frey-Martínez et al., 2006), which may also be controlled by the morphology of the basin itself (see Section 5.3.1). Synchronous with the compression of the basin sequence and the emplacement of the coherent sliding mass, the remolded slope sediments propagate as a mass flow along the lake floor, occasionally eroding and including the unconsolidated upper strata of the uplifted basin sequence (Fig. 11c). This implies that the propagation of the fold-and-thrust system was slightly faster than the mass flow, which, according to the literature, may range between 1 and 10 m s^{-1} (Talling et al., 2007; Iverson et al., 2010; Heerema et al., 2020). In the numerical simulation of St. Niklausen slide the coherent mass reached a maximum velocity of 6.5 m s^{-1} (Stoecklin et al., 2020). The shear band propagation could have happened with a velocity of the same order of magnitude, nevertheless, a precise quantification is not possible. Similar examples of a delayed mass flow eroding freshly deformed and up-lifted basin sediments are reported in the literature from lakes and fjords (Van Daele et al., 2013; Daxer et al., 2020), confirming that fold-and-thrust systems can develop very quickly.

The result of this slope instability is a MTD that consists of i) ~40–50% of deformed basin sediments (Table 2), which failed and formed an in situ fold-and-thrust system, and a variable percentage of ii) mass-slide deposit comprising the sliding coherent sediments derived from the upslope source area, and iii) mass-flow deposit, mainly consisting of remolded slope sediments with some incorporation of basin sediments. The model proposed in this study complements and refines the one proposed by Schnellmann et al. (2005) and other studies in marine environments (Watt et al., 2012; Joanne et al., 2013; Nugraha et al., 2020) as the geotechnical information acquired in Lake Lucerne and the high resolution of the data allowed a new quantitative assessment of the propagation model.

Watt et al. (2012) suggest that the fold-and-thrust structures in subaqueous deposits of volcanic debris avalanches are caused by the motion of an over-running flow, which induces undrained loading in the underlying sediments and consequent progressive deformation of the sequence. Even if the presence of a mass-flow deposit above the described frontally confined slides was potentially in agreement with the model proposed by Watt et al. (2012), this model can be excluded in Lake Lucerne because the mass-flow propagation occurred slightly later than the propagation of basin-plain deformation rather than being a preceding process. Furthermore, if the deformation was caused by over-running flow, the toe position of the mass-flow deposit and of the fold-and-thrust system should correspond, whereas our data indicate that the mass flow was propagating further out into the basin (i.e. Zinnen Baby slide, Fig. 6b).

In our model, the fold-and-thrust deformation structures are generated by the propagation within the basin sequence of the failing slope mass rather than by gravity spreading induced by loading on the lake floor (Schnellmann et al., 2005) or by impact of the failing mass (Lenz et al., 2019). These two processes would lead to an impact depression proximal to the base of the slope and to high circular compressional ridges (Van Daele et al., 2013; Daxer et al., 2020; Strasser et al., 2020) instead of an elongated area of numerous arcuate compressional ridges with defined lateral boundaries (Fig. 12). The impact-induced deformation model proposed by Lenz et al. (2019) involves excess pore

pressure at the basal shear surface with evidence of fluid-escape structures in seismic data, which are not visible in the data presented in this study. Furthermore, the impact of the failing mass on the basin sequence generates an immediate increase of pore pressure along the critical layer, and consequent synchronous and homogeneous deformation of the sediments above it. This is in disagreement with the above-described lower degree of sediment deformation in the toe region of the deposit, which strictly linked to the basinward propagation of the deformation front.

The mechanism for basin-plain deformation described here is similar to the one proposed by Huvenne et al. (2002), Joanne et al. (2013), and Nugraha et al. (2020), where the basin-sequence is deformed by a bulldozing highly remolded debris flow. Nevertheless, geotechnical data acquired in Lake Lucerne highlight that the driving mass kept its internal structure and strength and therefore cannot be considered as a debris flow but rather as a coherent sliding mass. The portion of slope material that got remolded during failure and propagation was not contributing to the basin-plain deformations but travelled above it as a mass flow.

5.3. Controlling factors

Our study area is characterized by the presence of frontally confined slides, assigned to the same trigger event and showing different styles and dimensions of deformation propagation into the basin-plain sediments, as well as of a section of unfailed slope adjacent to the failure scar areas. This makes the south-eastern slope of Küssnacht basin an ideal laboratory not only for studying the mechanism behind the soft-sediment deformation structures, but also for investigating the controlling factors for both slide propagation and slope stability.

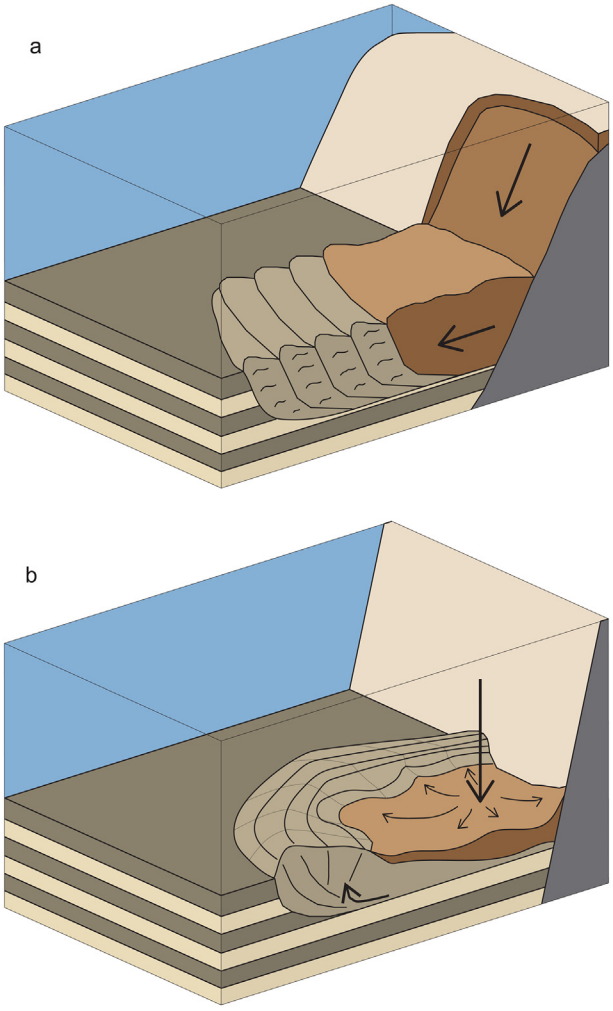

Fig. 12. Schematic model of (a) fold-and-thrust deformation structures generated by the propagation of a bulldozing sliding mass within the basin-plain sequence. As highlighted by seismic data the fold-and-thrust system is characterized by displaced packages of rather coherent and undisturbed basin sequence (highlighted by horizontal black lines), embedded in a chaotic-to-transparent seismic facies; (b) impact-induced deformation structures through gravity spreading.

5.3.1. Slide propagation: Zinnen slide vs Zinnen Baby slide

The two slides show many similarities, but the deformation structures were developing differently in the basin sedimentary sequence. In the Zinnen slide, the fold-and-thrust system unit has a total horizontal length of ~205 m, with the steep frontal thrust ~330 m away from the slope break. In the Zinnen Baby slide the ~60 m horizontally-long fold-and-thrust system stopped ~130 m from the slope break. Beyond the frontal thrust, two early-stage blind thrusts indicate that the deformation front started to propagate basinward along the decollement surface and mark the locations where the next thrusts would have formed (Nugraha et al., 2020). Furthermore, even considering the high volumetric difference of the failing material on the slope, there is a substantial difference in the propagation and deposition behavior of this material. In the Zinnen slide, ~75% of the failing mass was moving basinward as a coherent sliding mass (red area in Fig. 6a), pushing and deforming the basin-plain sediments, whereas the remaining 25% was propagating as a mass flow (yellow area in Fig. 6a). On the other hand, in the Zinnen Baby slide, just 36% of the failing material moved as a coherent mass, and 64% was deposited as mass flow (red and yellow area in Fig. 6b, respectively; Table 1).

As highlighted in Section 4.2.1, in front of the Zinnen slide, there is a glacial depression, clearly visible in the entire Holocene and upper Late Glacial basin sequence, the basinward margin of which prevented further propagation of the deformation front. On the other hand, in front of the Zinnen Baby slide the basin sequence consists of horizontal layers, with a planar decollement surface. The dip of the decollement surface is known to be a primary and critical factor in controlling the downslope propagation of a sliding mass. In particular, a steeper decollement surface facilitates the sliding process, making it easier to overcome the resistance to slip (Rowan et al., 2004). This could potentially explain the difference between the two slides, which otherwise have comparable settings (i.e. stratigraphic succession, slope gradient, depth of basal shear surface). After the first thrust was formed in the base-of-slope area of the Zinnen slide, the inclination change of the decollement surface at the glacial depression, provided the shear band with sufficient inertial energy to propagate further into the basin, enlarging the quasi-stable zone (Puzrin et al., 2016). The shear band propagation, and therefore the propagation of the fold-and-thrust system, stopped at the basinward margin of the depression. The more extended propagation of the deformation front in the Zinnen slide resulted in more accommodation space for the failing material to be deposited as a coherent mass at the base of the slope. In the Zinnen Baby slide, the deformation front started to propagate along the horizontal decollement surface, but stopped when the resistance of basin sediments was higher than the lateral compression stress of the coherent sliding mass (Frey-Martínez et al., 2006). This resulted in two blind thrusts, a higher percentage of sediments deposited as mass-flow deposit (Tables 1, 2) and in a single, slightly more developed frontal thrust, which is displacing the basin sequence of up to 2 m vertically, compared to 1.5 m in the Zinnen slide. This suggests that in the Zinnen Baby slide, the basin sediments between the base of the slope and the frontal thrust have been subjected to a higher level of compression, as confirmed by the higher lateral shortening and higher reduction in volume of the basin sequence with respect to a reconstructed pre-failure situation. The basin sequence has been horizontally shortened by 32% and 43% for the Zinnen slide and Zinnen Baby slide, respectively, with a reduction in volume of 15% and 25% (Table 3).

The higher buttress given by the horizontal sedimentary sequence at the base of the Zinnen Baby slope slowed down the propagation within

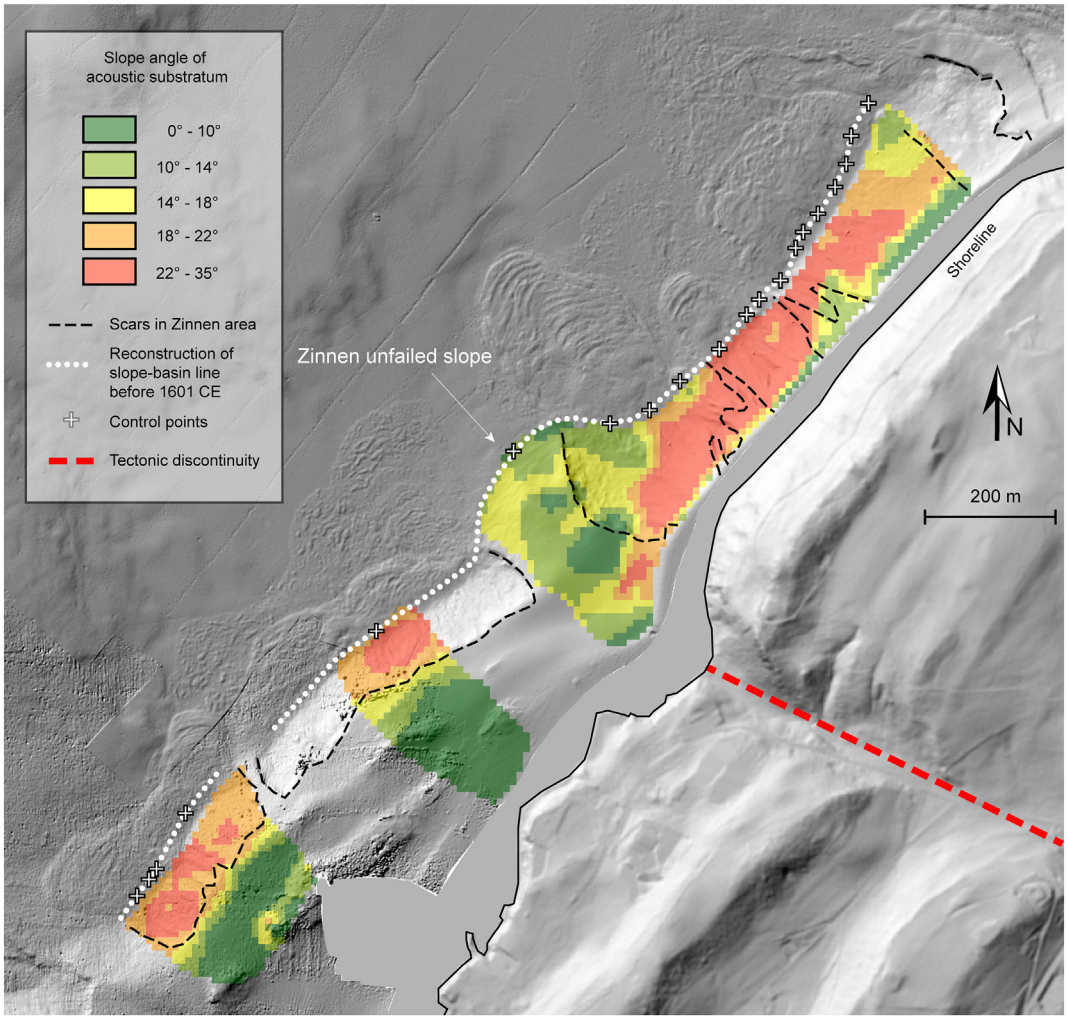

Fig. 13. Hillshade of the south-eastern slope of the Küssnacht basin with the slope angle map of the acoustic substratum (top of Glacial sediments). The slope angle map was generated by mapping the acoustic substratum in the seismic lines available (position of seismic lines used for the analysis is marked with control points). The figure highlights that the unfailed slope in the Küssnacht basin has a lower inclination of the gliding surface compared to the failed areas. In the failed portions of the slope, the gliding surface slope angle exceeded 14°. (For interpretation of the references to color in this figure, the reader is referred to the web version of this article.)

the basin-plain sequence of the coherent mass, which had less accommodation space for depositing at the base of the slope. This led to increased turbulence at the base of the slope between the failing material and the water column, and therefore to a higher water entrainment. A higher amount of failing material got remolded and underwent flow transformation into the evolving mass flow, explaining the higher percentage of material deposited as mass flow in the Zinnen Baby slide compared to the Zinnen slide (Tables 1, 2).

5.3.2. Slope stability: unfailed slope

As shown in the bathymetric data (Fig. 5), just a small section (~0.26 km^2) of the entire south-eastern slope of Küssnacht Basin did not collapse during the 1601 CE earthquake. This section is located in the central part of the slope, between the Zinnen slide described by Schnellmann et al. (2005) and the Zinnen slide discussed in the present study. As shown by short core and CPT data, it is characterized by a slope sequence that is highly comparable with sediments characterizing the nearby failed slopes. The slope angle map of the acoustic substratum (located at the top of the Glacial sediments; Fig. 13), can be approximated as the slope angle of the gliding surface due to the thin drape of unfailed Late Glacial sediments. The unfailed section of the slope has a lower inclination of the gliding surface with respect to the failed slopes where slope inclination is exceeding ~14°. This threshold is particularly clear for the slides south of the unfailed slope, where the headscarps formed on slope segments that steepened downwards beyond 14 and 18°. In the northern part of the basin, the headscarps are too shallow to be completely imaged on bathymetry and seismic data, but the scars show a mean slope angle of the gliding surface of 20°, whereas in the unfailed section, slope angles of stratigraphic-equivalent potential weak-layer surface never exceed 14°, with a mean value of 10°. This threshold is consistent with what has already been observed and confirmed by slope stability analysis in Lake Lucerne (Strasser et al., 2011) and in the nearby Lake Zurich (Strupler et al., 2018). In both lakes, most of the translational failures of the last ~5000 years are located on slopes with a mean slope angle between 10° and 25°, which are also the ones presently most prone to failure. Those slopes are gentle enough to allow sediment accumulation, and steep enough for an external trigger (i.e. earthquake) to generate shear stresses greater than the sediment shear strength (Strupler et al., 2018). The difference in slope gradient of the gliding surface in the unfailed slope is explained by a different sedimentation process generating the acoustic substratum that might be caused by a fault displacing the molasses bedrock (dashed red line in Fig. 13) forming on land a depression with a small inflow. In Glacial times, when the acoustic substratum was formed, this small stream was most likely a bigger glacial meltwater inlet so that the substratum of the unfailed slope area might have been an active delta fan. This assumption is also supported by the reconstruction of the slope-basin break before the 1601 CE earthquake (dotted white line in Fig. 13). The line shows a fan-

shaped curve in front of the unfailed slope, which is interpreted to be the superficial expression of the paleodelta below.

6. Conclusions

By using a multidisciplinary approach, we investigated outstanding examples of frontally confined slides in Lake Lucerne.

We present the following conclusions:

- The new data acquired in the Küssnacht Basin show that the south-eastern slope of the basin almost entirely collapsed during the 1601 CE earthquake, generating outstanding examples of frontally confined slides with a different propagation distance despite having similar height drops and slope angles.
- The high-resolution data allow confirming and further refining the earlier description of frontally confined MTDs by Schnellmann et al. (2005). These MTDs can be subdivided into three different units: i) mass-slide deposit, located at the base of the slope and consisting of slightly deformed slope sediments, ii) fold-and-thrust system, with far-reaching deformation structures within the basin-plain sequence, expressed on the lake floor as compressional ridges, and iii) an overlying mass-flow deposit, consisting mainly of highly remolded slope sediments.
- Deformed and thrusted basin sediments in the fold-and-thrust system show lower water contents, higher densities and higher absolute values of undrained shear strength with steeper increasing trends with depth when compared to the undisturbed sequence. This strengthening is caused by the lateral compression and compaction of high-plasticity sediments.
- We propose a new conceptual model, in which the destabilized slope sequence propagates basinward as two different bodies: a remolded mass, which propagates as mass flow on the lake floor, and a coherent sliding mass, which plows into the basin-plain sequence, generating the fold-and-thrust deformation structures. This process operates in conjunction with a shear band propagation, which starts in the slope and can further propagate in otherwise stable areas of the basin, generating laterally extensive basin-plain deformations.
- The fold-and-thrust structures developed following an in-sequence synchronous propagation, with the internal sediments showing higher deformation and compression.
- The mass flow is slightly delayed with respect to the propagation of the fold-and-thrust structures within the basin sequence, as indicated by the superficial erosion highlighted by short core analysis. Such new information on relative kinematics of genetically-linked but individually-evolving mass movement bodies documents that lake floor deformation in frontally confined slides occurs rapidly and should be considered in tsunami hazard assessments from subaquatic landslides.
- The topography of the basin and a subtle change in inclination (only ~2–3°) of the basal shear surface can affect the propagation and depositional behavior of frontally confined slides. The presence of a topographic depression in front of a destabilized slope can facilitate the propagation of the deformation front, resulting in more accommodation space for the slope sequence to be deposited as coherent mass at the base of the slope.
- The slope angle of the gliding surface is a main controlling factor in determining whether a slope stays stable during strong earthquake shaking, or whether it fails. During the 1601 CE earthquake, slides in the Küssnacht Basin exclusively took place in locations where the gliding surface was steeper than ~14°.

This study in Lake Lucerne supports and further refines, geophysically-based frontally confined slide emplacement models proposed in the lacustrine and marine realms (Huvenne et al., 2002; Schnellmann et al., 2005; Joanne et al., 2013; Nugraha et al., 2020), and further links rheological and geotechnical interpretation with the shear band propagation model proposed by numerical models (Puzrin et al., 2016; Stoecklin et al., 2020). The acquisition of CPT data in the undisturbed basin sequence and along the axis of the slide deposit represents a novelty in this field. These data were essential for quantifying the degree of deformation of the different units of the MTD and, therefore, for proposing the new conceptual model. The geotechnical observations gained further reliability by integrating the geophysical data, and found additional confirmation in outcrop-based studies of fold-and-thrust systems. In summary, this study highlights the potential of investigating easy-to-access lacustrine frontally confined slides for improving our understanding of subaqueous slides at the much larger scale of the marine realm.

Declaration of competing interest

The authors declare that they have no known competing financial interests or personal relationships that could have appeared to influence the work reported in this paper.

Acknowledgments

This work was funded by the European Union's Horizon 2020 - Research and Innovation Framework Programme under the H2020 Marie Skłodowska-Curie Actions grant agreement No 721403 - ITN-SLATE (Submarine Landslides and their impact on European continental margins). Flavio S. Anselmetti, Achim Kopf, and Sylvia Stegmann acknowledge funding from SNF-Sinergia (project number CRSII5_171017).

For logistical and technical support during Lake Lucerne campaigns, the authors would like to thank Alois Zwyssig and Eawag, Gauvain Wiemer, Katrina Kremer, and Steffen Hammerschmidt. Furthermore, all SLATE ESRs are thanked for the help during acquisition in September 2018, and Markus Erhardt from Medical University Innsbruck is thanked for acquisition of the CT scan data.

Maddalena Sammartini thanks the Marine Geotechnics group at MARUM, Bremen, for the help and support during the geotechnical tests, Barbara Schneider-Muntau for the help with the interpretation of the data, Marcel Ortler for the support with grain size analysis, and Anastasiia Shynkarenko for the interactions during CPT processing.

IHS Markit is acknowledged for their educational grant program providing the Kingdom seismic interpretation software.

We thank Massimo Moretti and Ian Alsop for their valuable and constructive reviews, and the editor Catherine Chagué for the helpful remarks and improvements of the manuscript.

Appendix A. Supplementary data

Supplementary data to this article can be found online at https://doi.org/10.1016/j.sedgeo.2021.105877.

References

Alsop, G.I., Marco, S., Weinberger, R., Levi, T., 2016. Sedimentary and structural controls on seismogenic slumping within mass transport deposits from the Dead Sea Basin. Sedimentary Geology 344, 71–90.

Alsop, G.I., Weinberger, R., Marco, S., 2018. Distinguishing thrust sequences in gravity-driven fold and thrust belts. Journal of Structural Geology 109, 99–119.

Alsop, G.I., Weinberger, R., Marco, S., Levi, T., 2019. Fold and thrust systems in mass-transport deposits around the Dead Sea Basin. In: Ogata, K., Festa, A., Pini, G.A. (Eds.), Submarine Landslides: Subaqueous Mass Transport Deposits From Outcrops to Seismic Profiles. AGU and John Wiley and Sons, Washington, pp. 139–153.

Alsop, G.I., Weinberger, R., Marco, S., Levi, T., 2020. Distinguishing coeval patterns of contraction and collapse around flow lobes in mass transport deposits. Journal of Structural Geology 134, 104013. https://doi.org/10.1016/j.jsg.2020.104013.

Badhani, S., Cattaneo, A., Dennielou, B., Leroux, E., Colin, F., Thomas, Y., Jouet, G., Rabineau, M., Droz, L., 2020. Morphology of retrogressive failures in the Eastern Rhône interfluve during the last glacial maximum (Gulf of Lions, Western Mediterranean). Geomorphology 351, 106894. https://doi.org/10.1016/j.geomorph.2019.106894.

BSI, 1990. BS 1377-2: Methods of Test for Soil for Civil Engineering Purposes. British Standard Institution, London (36 pp.).

BSI, 2015. BS 5930:2015: Code of Practice for Ground Investigations. British Standard Institution, London (328 pp.).

Bull, S., Cartwright, J.A., 2020. Line length balancing to evaluate multi-phase submarine landslide development: an example from the Storegga Slide, Norway. In: Georgiopoulou, A., Amy, L.A., Benetti, S., Chaytor, J.D., Clare, M.A., Gamboa, D., Haughton, P.D.W., Moernaut, J., Mountjoy, J.J. (Eds.), Subaqueous Mass Movements and Their Consequences: Advances in Process Understanding, Monitoring and Hazard Assessments. Geological Society, London, Special Publications vol. 500, pp. 531–549.

Bull, S., Cartwright, J.A., Huuse, M., 2009. A review of kinematic indicators from mass-transport complexes using 3D seismic data. Marine and Petroleum Geology 26, 1132–1151.

Callot, P., Odonne, F., Sempere, T., 2008. Liquification and soft-sediment deformation in a limestone megabreccia: the Ayabacas giant collapse, Cretaceous, southern Peru. Sedimentary Geology 212, 49–69.

Cardona, S., Wood, L.J., Day-Stirrat, R.J., Moscardelli, L., 2016. Fabric development and pore-throat reduction in a mass-transport deposit in the Jubilee Gas Field, Eastern Gulf of Mexico: consequences for the sealing capacity of MTDs. In: Lamarche, G., Mountjoy, J.J., Bull, S., Hubble, T., Krastel, S., Lane, E., Micallef, A., Moscardelli, L., Mueller, C., Pecher, I., Woelz, S. (Eds.), Submarine Mass Movements and Their Consequences: 7th International Symposium. Advances in Natural and Technological Hazard Research vol. 41. Springer, Cham, pp. 27–37.

Carter, L., Gavey, R., Talling, P.J., Liu, J.T., 2014. Insights into submarine geohazards from breaks in subsea telecommunication cables. Oceanography 27, 58–67.

Clare, M.A., Chaytor, J., Dabson, O., Gamboa, D., Georgiopoulou, A., Eady, H., Hunt, J., Jackson, C., Katz, O., Krastel, S., Leon, R., Micallef, A., Moernaut, J., Moriconi, R., Moscardelli, L., Mueller, C., Normandeau, A., Patacci, M., Steventon, M., Urlaub, M., Voelker, D., Wood, L., Zane, J., 2018. A consistent global approach for the morphomet-ric characterization of subaqueous landslides. In: Lintern, D.G., Mosher, D.C., Moscardelli, L.G., Bobrowsky, P.T., Campbell, C., Chaytor, J., Clague, J., Georgiopoulou, A., Lajeunesse, P., Normandeau, A., Piper, D., Scherwath, M., Stacey, C., Turmel, D. (Eds.), Subaqueous Mass Movements and Their Consequences: Assessing Geohazards, Environmental Implications and Economic Significance of Subaqueous Landslides. Geological Society, London, Special Publications vol. 477, pp. 455–477.

Clare, M.A., Vardy, M.E., Cartigny, M.J., Talling, P.J., Himsworth, M.D., Dix, J.K., Harris, J.M., Whitehouse, R.J., Belal, M., 2017. Direct monitoring of active geohazards: emerging geophysical tools for deep-water assessments. Near Surface Geophysics 15, 427–444.

Craig, R.F., 2004. Craig's Soil Mechanics. Taylor & Francis Group, London (464 pp.).

Damuth, J.E., 1980. Use of high-frequency (3.5–12 kHz) echograms in the study of near-bottom sedimentation processes in the deep-sea: a review. Marine Geology 38, 51–75.

Daxer, C., Sammartini, M., Molenaar, A., Piechl, T., Strasser, M., Moernaut, J., 2020. Morphology and spatio-temporal distribution of lacustrine mass-transport deposits in Wörthersee, Eastern Alps, Austria. In: Georgiopoulou, A., Amy, L.A., Benetti, S., Chaytor, J.D., Clare, M.A., Gamboa, D., Haughton, P.D.W., Moernaut, J., Mountjoy, J.J. (Eds.), Subaqueous Mass Movements and Their Consequences: Advances in Process Understanding, Monitoring and Hazard Assessments. Geological Society, London, Special Publications vol. 500, pp. 235–254.

Deutsches Institut für Normung, 1999. Baugrund – Untersuchung von Bodenproben – Eindimensionaler Kompressionsversuch. DIN-Norm 18135: 1999-06. Beuth, Berlin (38 pp., in German).

Deutsches Institut für Normung, 2002. Baugrund – Untersuchung von Bodenproben – Bestimmung der Scherfestigkeit. DIN-Norm 18137-3. Beuth, Berlin (33pp., in German).

Farrell, S.G., 1984. A dislocation model applied to slump structures, Ainsa Basin, South Central Pyrenees. Journal of Structural Geology 6, 727–736.

Finckh, P., Kelts, K., Lambert, A., 1984. Seismic stratigraphy and bedrock forms in perialpine lakes. Geological Society of America Bulletin 95, 1118–1128.

Ford, J., Camerlenghi, A., 2020. Geostatistical characterization of internal structure of mass-transport deposits from seismic reflection images and borehole logs. Geophysical Journal International 221, 318–333.

Frey-Martínez, J., Cartwright, J., James, D., 2006. Frontally confined versus frontally emergent submarine landslides: a 3D seismic characterisation. Marine and Petroleum Geology 23, 585–604.

Gamberi, F., Rovere, M., Marani, M., 2011. Mass-transport complex evolution in a tectonically active margin (Gioia Basin, Southeastern Tyrrhenian Sea). Marine Geology 279, 98–110.

Gatter, R., Clare, M.A., Hunt, J.E., Watts, M., Madhusudhan, B.N., Talling, P.J., Huhn, K., 2020. A multi-disciplinary investigation of the AFEN Slide: the relationship between contourites and submarine landslides. In: Georgiopoulou, A., Amy, L.A., Benetti, S., Chaytor, J.D., Clare, M.A., Gamboa, D., Haughton, P.D.W., Moernaut, J., Mountjoy, J.J. (Eds.), Subaqueous Mass Movements and Their Consequences: Advances in Process Understanding, Monitoring and Hazard Assessments. Geological Society, London, Special Publications vol. 500, pp. 173–193.

Glimsdal, S., L'Heureux, J.S., Harbitz, C.B., Løvholt, F., 2016. The 29th January 2014 submarine landslide at Statland, Norway—landslide dynamics, tsunami generation, and run-up. Landslides 13, 1435–1444.

Harbitz, C.B., Løvholt, F., Bungum, H., 2014. Submarine landslide tsunamis: how extreme and how likely? Natural Hazards 72, 1341–1374.

Heerema, C.J., Talling, P.J., Cartigny, M.J., Paull, C.K., Bailey, L., Simmons, S.M., Parson, D.R., Clare, M.A., Gwiazda, R., Lundsten, E., Anderson, K., Maier, K.L., Xu, J.P., Sumner, E.J., Rosenberger, K., Gales, J., McGann, M., Carter, L., Pope, E., 2020. What determines the downstream evolution of turbidity currents? Earth and Planetary Science Letters 532, 116023. https://doi.org/10.1016/j.epsl.2019.116023.

Hilbe, M., Anselmetti, F.S., 2014. Signatures of slope failures and river-delta collapses in a perialpine lake (Lake Lucerne, Switzerland). Sedimentology 61, 1883–1907.

Hilbe, M., Anselmetti, F.S., Eilertsen, R.S., Hansen, L., Wildi, W., 2011. Subaqueous morphology of Lake Lucerne (Central Switzerland): implications for mass movements and glacial history. Swiss Journal of Geosciences 104, 425–443.

Hungr, O., Leroueil, S., Picarelli, L., 2014. The Varnes classification of landslide types, an update. Landslides 11, 167–194.

Huvenne, V.A., Croker, P.F., Henriet, J.P., 2002. A refreshing 3D view of an ancient sediment collapse and slope failure. Terra Nova 14, 33–40.

Ikari, M.J., Kopf, A.J., 2015. The role of cohesion and overconsolidation in submarine slope failure. Marine Geology 369, 153–161.

Infante, D.J.U., Martinez, G.M.A., Arrua, P.A., Eberhardt, M., 2016. Shear strength behavior of different geosynthetic reinforced soil structure from direct shear test. International Journal of Geosynthetics and Ground Engineering 2, 1–16.

Iverson, R.M., Logan, M., LaHusen, R.G., Berti, M., 2010. The perfect debris flow? Aggregated results from 28 large-scale experiments. Journal of Geophysical Research: Earth Surface 115, F03005. https://doi.org/10.1029/2009JF001514.

Jackson, C.A., 2011. Three-dimensional seismic analysis of megaclast deformation within a mass transport deposit; implications for debris flow kinematics. Geology 39, 203–206.

Joanne, C., Lamarche, G., Collot, J.Y., 2013. Dynamics of giant mass transport in deep submarine environments: the Matakaoa Debris Flow, New Zealand. Basin Research 25, 471–488.

Keller, B., 2017. Massive rock slope failure in Central Switzerland: history, geologic–geomorphological predisposition, types and triggers, and resulting risks. Landslides 14, 1633–1653.

Kelts, K.R., 1978. Geological and Sedimentary Evolution of Lakes Zurich and Zug, Switzerland. ETH Zurich, Zurich (Ph.D. thesis).

Kremer, K., Wirth, S.B., Reusch, A., Fäh, D., Bellwald, B., Anselmetti, F.S., Girardclos, S., Strasser, M., 2017. Lake-sediment based paleoseismology: Limitations and perspectives from the Swiss Alps. Quaternary Science Reviews 168, 1–18.

Laberg, J.S., Strasser, M., Alves, T.M., Gao, S., Kawamura, K., Kopf, A., Moore, G.F., 2017. Internal deformation of a muddy gravity flow and its interaction with the seafloor (site C0018 of IODP Expedition 333, Nankai Trough, SE Japan). Landslides 14, 849–860.

Lastras, G., Canals, M., Amblas, D., Ivanov, M., Dennielou, B., Droz, L., Akhmetzhanov, A., 2006. Eivissa slides, western Mediterranean Sea: morphology and processes. Geo-Marine Letters 26, 225–233.

Lastras, G., Canals, M., Hughes-Clarke, J.E., Moreno, A., De Batist, M., Masson, D.G., Cochonat, P., 2002. Seafloor imagery from the BIG'95 debris flow, western Mediterranean. Geology 30, 871–874.

Lenz, B.L., Sawyer, D.E., Phrampus, B., Davenport, K., Long, A., 2019. Seismic imaging of seafloor deformation induced by impact from large submarine landslide blocks, offshore Oregon. Geosciences 9, 10. https://doi.org/10.3390/geosciences9010010.

Locat, J., Leroueil, S., Locat, A., Lee, H., 2014. Weak layers: their definition and classification from a geotechnical perspective. In: Krastel, S., Behrmann, J.H., Völker, D., Stipp, M., Berndt, C., Urgeles, R., Chaytor, J., Huhn, K., Strasser, M., Harbitz, C.B. (Eds.), Submarine Mass Movements and Their Consequences: 6th International Symposium. Advances in Natural and Technological Hazard Research vol. 37. Springer, Cham, pp. 3–12.

Løvholt, F., Glimsdal, S., Harbitz, C.B., 2020. On the landslide tsunami uncertainty and hazard. Landslides 17, 2301–2315.

Lunne, T., Robertson, P.K., Powell, J.J., 1997. Cone Penetration Testing in Geotechnical Practice. Taylor & Francis Group, London (352 pp.).

Martinsen, O., 1994. Mass movements. In: Maltman, A. (Ed.), The Geological Deformation of Sediments. Springer, Dordrecht, pp. 127–165.

Martinsen, O.J., Bakken, B., 1990. Extensional and compressional zones in slumps and slides in the Namurian of County Clare, Ireland. Journal of the Geological Society 147, 153–164.

Masson, D.G., Harbitz, C.B., Wynn, R.B., Pedersen, G., Løvholt, F., 2006. Submarine landslides: processes, triggers and hazard prediction. Philosophical Transactions of the Royal Society A: Mathematical, Physical and Engineering Sciences 364, 2009–2039.

Masson, D.G., Watts, A.B., Gee, M.J.R., Urgeles, R., Mitchell, N.C., Le Bas, T.P., Canals, M., 2002. Slope failures on the flanks of the western Canary Islands. Earth-Science Reviews 57, 1–35.

Moernaut, J., De Batist, M., 2011. Frontal emplacement and mobility of sublacustrine landslides: results from morphometric and seismostratigraphic analysis. Marine Geology 285, 29–45.

Moernaut, J., Wiemer, G., Kopf, A., Strasser, M., 2020. Evaluating the sealing potential of young and thin mass-transport deposits: Lake Villarrica, Chile. In: Georgiopoulou, A., Amy, L.A., Benetti, S., Chaytor, J.D., Clare, M.A., Gamboa, D., Haughton, P.D.W., Moernaut, J., Mountjoy, J.J. (Eds.), Subaqueous Mass Movements and Their Consequences: Advances in Process Understanding, Monitoring and Hazard Assessments. Geological Society, London, Special Publications vol. 500, pp. 129–146.

Mohrig, D., Marr, J.G., 2003. Constraining the efficiency of turbidity current generation from submarine debris flows and slides using laboratory experiments. Marine and Petroleum Geology 20, 883–899.

Moscardelli, L., Wood, L., 2008. New classification system for mass transport complexes in offshore Trinidad. Basin Research 20, 73–98.

Mosher, D.C., Moran, K., Hiscott, R.N., 1994. Late Quaternary sediment, sediment mass flow processes and slope stability on the Scotian Slope, Canada. Sedimentology 41, 1039–1061.

Mosher, D.C., Moscardelli, L., Shipp, R.C., Chaytor, J.D., Baxter, C.D., Lee, H.J., Urgeles, R., 2010. Submarine mass movements and their consequences. In: Mosher, D.C., Shipp, R.C., Moscardelli, L., Chaytor, J.D., Baxter, C.D.P., Lee, H.J., Urgeles, R. (Eds.), Submarine Mass Movements and Their Consequences. Advances in Natural and Technological Hazard Research vol. 28. Springer, Dordrecht, pp. 1–8.

Mountjoy, J.J., Georgiopoulou, A., Chaytor, J., Clare, M.A., Gamboa, D., Moernaut, J., 2020. Subaqueous mass movements in the context of observations of contemporary slope

failure. In: Georgiopoulou, A., Amy, L.A., Benetti, S., Chaytor, J.D., Clare, M.A., Gamboa, D., Haughton, P.D.W., Moernaut, J., Mountjoy, J.J. (Eds.), Subaqueous Mass Movements and Their Consequences: Advances in Process Understanding, Monitoring and Hazard Assessments. Geological Society, London, Special Publications vol. 500, pp. 1–12.

Normandeau, A., Campbell, D.C., Piper, D.J., Jenner, K.A., 2019. New evidence for a major late Quaternary submarine landslide on the external western levee of Laurentian Fan. In: Lintern, D.G., Mosher, D.C., Moscardelli, L.G., Bobrowsky, P.T., Campbell, C., Chaytor, J., Clague, J., Georgiopoulou, A., Lajeunesse, P., Normandeau, A., Piper, D., Scherwath, M., Stacey, C., Turmel, D. (Eds.), Subaqueous Mass Movements and Their Consequences: Assessing Geohazards, Environmental Implications and Economic Significance of Subaqueous Landslides. Geological Society, London, Special Publications vol. 477, pp. 377–387.

Nugraha, H.D., Jackson, C.A., Johnson, H.D., Hodgson, D.M., 2020. Lateral variability in strain along a mass-transport deposit (MTD) toewall: a case study from the Makassar Strait, offshore Indonesia. Journal of the Geological Society 177, 1261–1279.

Ogata, K., Pogačnik, Ž., Pini, G.A., Tunis, G., Festa, A., Camerlenghi, A., Rebesco, M., 2014. The carbonate mass transport deposits of the Paleogene Friuli Basin (Italy/Slovenia): internal anatomy and inferred genetic processes. Marine Geology 356, 88–110.

Okkels, N., 2019. Modern guidelines for classification of fine soils. The XVII European Conference on Soil Mechanics and Geotechnical Engineering, Reykjavik, Iceland https://doi.org/10.32075/17ECSMGE-2019-0651.

Pickering, K.T., Corregidor, J., 2005. Mass transport complexes and tectonic control on confined basin-floor submarine fans, Middle Eocene, south Spanish Pyrenees. In: Hodgson, D.M., Flint, S.S. (Eds.), Submarine Slope Systems: Processes and Products. Geological Society, London, Special Publications vol. 244, pp. 51–74.

Pickering, K.T., Hiscott, R.N., 2016. Deep Marine Systems. Processes, Deposits, Environments, Tectonics and Sedimentation. AGU and John Wiley & Sons, Chichester (657 pp.).

Piper, D.J., Cochonat, P., Morrison, M.L., 1999. The sequence of events around the epicentre of the 1929 Grand Banks earthquake: initiation of debris flows and turbidity current inferred from sidescan sonar. Sedimentology 46, 79–97.

Piper, D.J., Pe-Piper, G., Ingram, S.C., 2004. Early Cretaceous sediment failure in the southwestern Sable Subbasin, offshore Nova Scotia. AAPG Bulletin 88, 991–1006.

Prior, D.B., Bornhold, B.D., Johns, M.W., 1984. Depositional characteristics of a submarine debris flow. The Journal of Geology 92, 707–727.

Puzrin, A.M., Germanovich, L.N., Friedli, B., 2016. Shear band propagation analysis of submarine slope stability. Géotechnique 66, 188–201.

Puzrin, A.M., Gray, T.E., Hill, A.J., 2015. Significance of the actual nonlinear slope geometry for catastrophic failure in submarine landslides. Proceedings of the Royal Society A: Mathematical, Physical and Engineering Sciences 471, 20140772. https://doi.org/10.1098/rspa.2014.0772.

Rowan, M.G., Peel, F.J., Vendeville, B.C., 2004. Gravity-driven fold belts on passive margins. In: McClay, K.R. (Ed.), Thrust Tectonics and Hydrocarbon Systems. AAPG Memoir vol. 82. AAPG, Tulsa, pp. 157–182.

Sammartini, M., Moernaut, J., Anselmetti, F.S., Hilbe, M., Lindhorst, K., Praet, N., Strasser, M., 2019. An atlas of mass-transport deposits in lakes. In: Ogata, K., Festa, A., Pini, G.A. (Eds.), Submarine Landslides: Subaqueous Mass Transport Deposits From Outcrops to Seismic Profiles. AGU and John Wiley and Sons, Washington, pp. 201–226.

Schnellmann, M., Anselmetti, F.S., Giardini, D., McKenzie, J.A., 2005. Mass movement-induced fold-and-thrust belt structures in unconsolidated sediments in Lake Lucerne (Switzerland). Sedimentology 52, 271–289.

Schnellmann, M., Anselmetti, F.S., Giardini, D., Mckenzie, J.A., 2006. 15,000 years of mass-movement history in Lake Lucerne: implications for seismic and tsunami hazards. Eclogae Geologicae Helvetiae 99, 409–428.

Schnellmann, M., Anselmetti, F.S., Giardini, D., McKenzie, J.A., Ward, S.N., 2002. Prehistoric earthquake history revealed by lacustrine slump deposits. Geology 30, 1131–1134.

Schwab, W.C., Lee, H.J., Twichell, D.C., Locat, J., Nelson, C.H., McArthur, W.G., Kenyon, N.H., 1996. Sediment mass-flow processes on a depositional lobe, outer Mississippi Fan. Journal of Sedimentary Research 66, 916–927.

Shanmugam, G., Wang, Y., 2015. The landslide problem. Journal of Palaeogeography 4, 109–166.

Stegmann, S., Mörz, T., Kopf, A., 2006. Initial results of a new free fall-cone penetrometer (FF-CPT) for geotechnical in situ characterisation of soft marine sediments. Norwegian Journal of Geology/Norsk Geologisk Forening 86, 199–208.

Stegmann, S., Strasser, M., Anselmetti, F.S., Kopf, A., 2007. Geotechnical in situ characterization of subaquatic slopes: the role of pore pressure transients versus frictional strength in landslide initiation. Geophysical Research Letters 34, L07607. https://doi.org/10.1029/2006GL029122.

Steiner, A., Kopf, A.J., L'Heureux, J.S., Kreiter, S., Stegmann, S., Haflidason, H., Moerz, T., 2014. In situ dynamic piezocone penetrometer tests in natural clayey soils—a reappraisal of strain-rate corrections. Canadian Geotechnical Journal 51, 272–288.

Stewart, S.A., Argent, J.D., 2000. Relationship between polarity of extensional fault arrays and presence of detachments. Journal of Structural Geology 22, 693–711.

Stoecklin, A., Trapper, P., Puzrin, A.M., 2020. Controlling factors for post-failure evolution of subaqueous landslides. Géotechnique, 1–14 https://doi.org/10.1680/jgeot.19.P.230.

Strasser, M., 2008. Quantifying Late Quaternary Natural Hazards in Swiss Lakes: Subaquatic Landslides, Slope Stability Assessments, Paleoseismic Reconstructions and Lake Outbursts. ETH Zurich, Zurich (Ph.D. thesis).

Strasser, M., Berberich, T., Fabbri, S., Hilbe, M., Huang, J.S., Lauterbach, S., Ortler, M., Rechschreiter, H., Brauer, A., Anselmetti, F., Kowarik, K., 2020. Geomorphology and event-stratigraphy of recent mass-movement processes in Lake Hallstatt (UNESCO World Heritage Cultural Landscape, Austria). In: Georgiopoulou, A., Amy, L.A., Benetti, S., Chaytor, J.D., Clare, M.A., Gamboa, D., Haughton, P.D.W., Moernaut, J., Mountjoy, J.J. (Eds.), Subaqueous Mass Movements and their Consequences: Advances in Process Understanding, Monitoring and Hazard Assessments. Geological Society, London, Special Publications vol. 500, pp. 405–426.

Strasser, M., Hilbe, M., Anselmetti, F.S., 2011. Mapping basin-wide subaquatic slope failure susceptibility as a tool to assess regional seismic and tsunami hazards. Marine Geophysical Research 32, 331–347.

Strasser, M., Stegmann, S., Bussmann, F., Anselmetti, F.S., Rick, B., Kopf, A., 2007. Quantifying subaqueous slope stability during seismic shaking: Lake Lucerne as model for ocean margins. Marine Geology 240, 77–97.

Strupler, M., Danciu, L., Hilbe, M., Kremer, K., Anselmetti, F.S., Strasser, M., Wiemer, S., 2018. A subaqueous hazard map for earthquake-triggered landslides in Lake Zurich, Switzerland. Natural Hazards 90, 51–78.

Strupler, M., Hilbe, M., Anselmetti, F.S., Kopf, A.J., Fleischmann, T., Strasser, M., 2017. Probabilistic stability evaluation and seismic triggering scenarios of submerged slopes in Lake Zurich (Switzerland). Geo-Marine Letters 37, 241–258.

Talling, P.J., Wynn, R.B., Masson, D.G., Frenz, M., Cronin, B.T., Schiebel, R., Akhmetzhanov, A.M., Dallmeier-Tiessen, S., Benetti, S., Weaver, P.P.E., Georgiopoulou, A., Zühlsdorff, C., Amy, L.A., 2007. Onset of submarine debris flow deposition far from original giant landslide. Nature 450, 541–544.

Terzaghi, K., Peck, R.B., Mesri, G., 1996. Soil Mechanics in Engineering Practice. John Wiley & Sons, New York (592 pp.).

Trincardi, F., Argnani, A., 1990. Gela submarine slide: a major basin-wide event in the Plio-Quaternary foredeep of Sicily. Geo-Marine Letters 10, 13–21.

Urgeles, R., Camerlenghi, A., 2013. Submarine landslides of the Mediterranean Sea: trigger mechanisms, dynamics, and frequency-magnitude distribution. Journal of Geophysical Research: Earth Surface 118, 2600–2618.

Van Daele, M., Meyer, I., Moernaut, J., De Decker, S., Verschuren, D., De Batist, M., 2017. A revised classification and terminology for stacked and amalgamated turbidites in environments dominated by (hemi) pelagic sedimentation. Sedimentary Geology 357, 72–82.

Van Daele, M., Versteeg, W., Pino, M., Urrutia, R., De Batist, M., 2013. Widespread deformation of basin-plain sediments in Aysén fjord (Chile) due to impact by earthquake-triggered, onshore-generated mass movements. Marine Geology 337, 67–79.

Watt, S.F., Karstens, J., Micallef, A., Berndt, C., Urlaub, M., Ray, M., Desai, A., Sammartini, M., Klaucke, I., Böttner, C., Day, S., Downes, H., Kühn, M., Elger, J., 2019. From catastrophic collapse to multi-phase deposition: Flow transformation, seafloor interaction and triggered eruption following a volcanic-island landslide. Earth and Planetary Science Letters 517, 135–147.

Watt, S.F., Talling, P.J., Vardy, M.E., Masson, D.G., Henstock, T.J., Hühnerbach, V., Minshull, T.A., Urlaub, M., Lebas, E., Le Friant, A., Berndt, C., Crutchley, G.J., Karstens, J., 2012. Widespread and progressive seafloor-sediment failure following volcanic debris avalanche emplacement: landslide dynamics and timing offshore Montserrat, Lesser Antilles. Marine Geology 323, 69–94.

Williams, R., Rowley, P., Garthwaite, M.C., 2019. Reconstructing the Anak Krakatau flank collapse that caused the December 2018 Indonesian tsunami. Geology 47, 973–976.

Wood, D.M., 1985. Some fall-cone tests. Géotechnique 35, 64–68.

Yilmaz, Ö., 2001. Seismic Data Analysis: Processing, Inversion, and Interpretation of Seismic Data. Society of Exploration Geophysicists, Tulsa (2065 pp.).